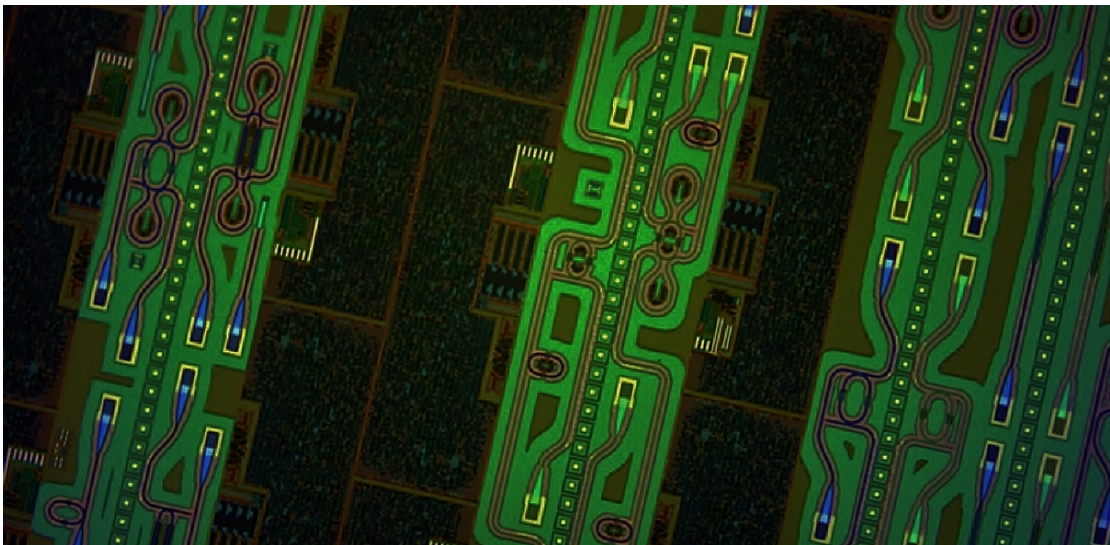




UNIVERSITAT POLITÈCNICA DE CATALUNYA

BACHELOR'S THESIS IN ENGINEERING PHYSICS

Quantum integrated photonics



Author:
Josep Maria
Fargas Cabanillas

Advisor:
Prof. Milos Popovic

Co-Advisor:
Dr. Jose Antonio Lazaro Villa

Nanophotonic Systems Laboratory

Boulder, CO

May 2016

Abstract

For many years scientist and engineers have used complex photonic set ups on large optical tables to perform quantum experiments. The problem is while the experiments are getting more and more complex the set ups are getting more and more complex too. Integration on chip has allowed the implementation of many optical devices in less than a few square millimeters. Also, quantum integrated photonics has become more popular in recent years. This technology gives a way to perform quantum experiments in a chip. Some people are really pessimistic about integrated quantum photonics due to losses and other complicated problems that have to be solved.

In this thesis, we provide an overview in the field of integrated quantum photonics, presenting how to implement quantum circuits going from the generic formulation to the specific implementation in this platform. We also will see the basic building blocks for future quantum information processing and communication technologies. These blocks include the generation, manipulation and detection of quantum states of light. Specifically we will focus on how to manipulate quantum light on chip. After that we will focus on the understanding of 2x2 couplers. Those elements are keys to perform quantum integrated photonics. Finally we will provide a novel design for a short broadband 2x2 coupler.

Dedicated to my brother and my sister: Dani and Gemma

Acknowledgements

First of all I want to acknowledge all the people that helped me and support me in this journey. I want to thank my advisor Prof. Milos Popovic for his guidance during my project. He has help me and gave me key advises. I would like to thank my co. advisor Jose Antonio Lazaro for all the support from Spain. With out both of you this thesis would not be possible. I would like to acknowledge all the members of the lab, Imbert, Yangyang, Savvy, Mark, Nathan, Yossi, Hayk and specially Cale. For helping me and for their patience with my infinite nonsense questions. I will want to say thanks to my family an my friends in Boulder specially to Edu, Alberto, Carlos, Diego, Pere, Clara, Savina, Maria, Sebastian to give me support in my stance in Colorado. Finally I will like to acknowledge my sponsors: Fundacio Balsells, Nanophotonics LAB and CFIS. With out their founding this adventure would not be possible.

Contents

Abstract	iii
Acknowledgements	vii
1 Introduction	1
2 A way to quantum integrated photonics	3
2.1 Brief foundations of quantum mechanics	3
2.1.1 States	4
2.1.2 Measurements	5
2.1.3 Time evolution	6
2.1.4 Heisenberg’s uncertainty principle	6
2.1.5 Qubits	6
2.2 Linear optics quantum computing	7
2.2.1 Path-Encoded Qubits	7
2.2.2 Unitary operations transformation	8
2.3 Puzzle pieces	9
2.3.1 Quantum beam splitter	9
2.3.2 Phase shifter and MZI	10
2.3.3 Single photon source	10
introduction	10
Theory of SFWM Sources	11
2.3.4 Single photon detector	11
Introduction	11
Application details	12
State of the art	14
2.4 Quantum algorithms applied to integrated optics	14
2.4.1 The CNOT gate	15
2.4.2 Measured based quantum computation	16
2.4.3 Linear optical controlled-NOT gate	17
3 Designing a broadband beam splitter	19
3.1 Slab waveguide	19
3.2 3D waveguides	23
3.3 Coupled mode theory	27
3.4 Directional Coupler	31
3.4.1 Directional Coupler: CMT approach	31
3.4.2 Directional Coupler: FDTD approach	34
3.4.3 Mach-Zehnder interferometer	38
3.5 Adiabatic coupler	41
3.6 Zero Xtalk coupler	44
4 Conclusions	53

Chapter 1

Introduction

The main aim of this thesis is to explore the viability and application of integrated quantum photonics. This thesis has two parts; chapter 2 and chapter 3. Chapter 2 is a bibliographic research about quantum integrated photonics and chapter 3 is a device level novel design of a 2x2 beam splitter.

Since we want this thesis to be self contained we will first introduce the foundations of quantum mechanics in section 2.1. Then we will see how we can specifically implement quantum mechanics on integrated photonics in section 2.2. If we divide a quantum integrated photonic circuit in different components we can distinguish at least three pieces: single photon sources, single photon detectors and Mach-Zehnder interferometers. We will see an overview of those three in section 2.3. Finally in section 2.4 we will see how to do quantum integrated computing on chip. We will realize that we need to add feedforward to be able to do quantum computing on chip.

In chapter 3 we will study the different ways to design a 2x2 beam splitter. In sections 3.1 and 3.1 we will start by the basic Electromagnetic theory for waveguide structures. Then we will derive coupled mode theory (CMT) in section 3.3. This theory is really useful to understand coupling between waveguides. CMT will be key to understand the directional coupler and the adiabatic coupler. We will see in detail the directional coupler in section 3.4 and the adiabatic coupler in section 3.5. We will simulate such devices using numerical tools. Most of my work is theoretical supported with simulations, however I had the opportunity to measure some Mach-Zehnder interferometers on chip so in section 3.4.3 we will see those results. Finally in section 3.6 we will explore a complete novel way to design 2x2 beam splitters.

Chapter 2

A way to quantum integrated photonics

It doesn't matter how beautiful your theory is, it doesn't matter how smart you are. If it doesn't agree with experiment, it's wrong.

Richard Feynman

2.1 Brief foundations of quantum mechanics

We can feel and sense a classical world. We know for sure that if we throw a ball it is going to do a parabolic trajectory. Newton's laws and Maxwell's equations rule the world. But is it really true?, during the 20th century, it became obvious that classical physics does not provide a complete vision of the world. The first evidences were the black body radiation and the photoelectric effect. Such effects can not be explained by a classical model. During the last century Planck, Bohr, Einstein, Schrödinger, Dirac, de Broglie, Feynman, Zurek and many others developed the theory of quantum mechanics, which explain perfectly the phenomena happening at the atomic-scale.

The creation of this theory broke completely the way to understand the nature. We have to assume some natural behavior which we are not use to experience daily. In particular, quantum mechanics assume that physical system is not well-defined until measured. For example a particle can be in two places at the same time until we measure and discover the position of the particle. In quantum mechanics there exists a mathematical object called a wavefunction which describes the system. This mathematical object contains all the information of the system. However this information can only be extracted in a probabilistic sense. Quantum mechanics also predicts new phenomena, such as entanglement and nonlocality, which are far away from our live experience. However this effects can be observed in nanoscale systems such as single atoms, electrons, and photons.

Quantum systems are very fragile. They like to be isolated from the environment. If they interact with the environment the quantum behavior leaks away and ends up disappearing. This effect is called decoherence and is the reason we can not experiment quantum mechanics in real life [1].

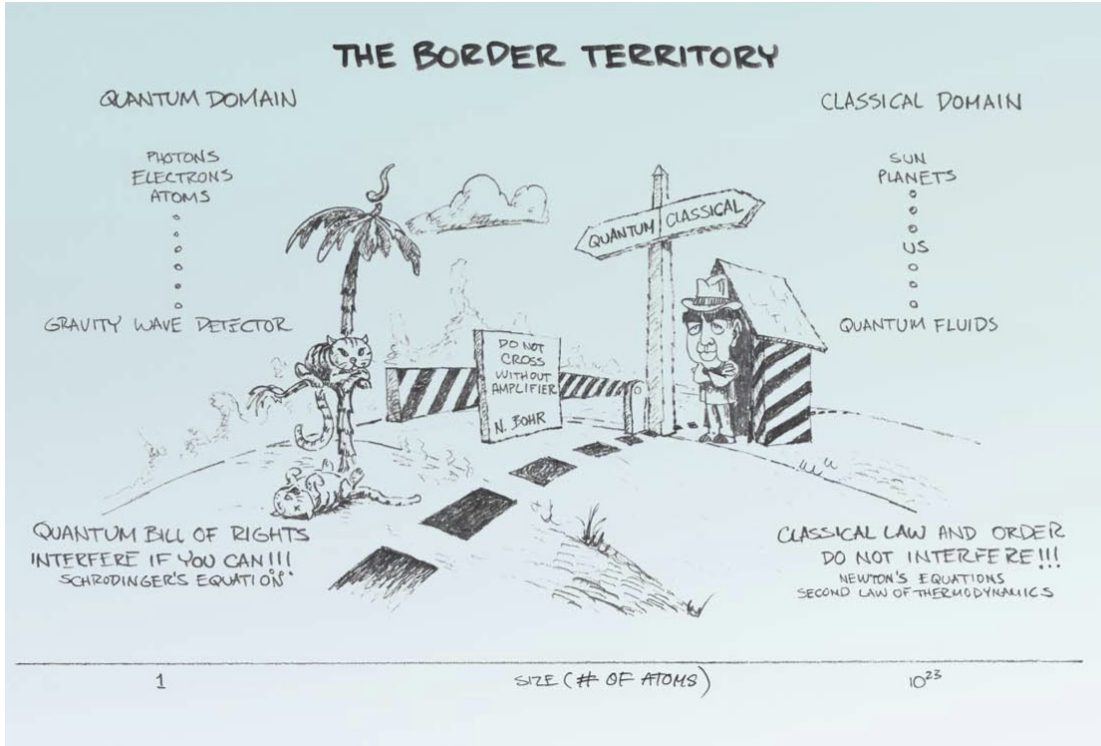


FIGURE 2.1: Artistic understanding of quantum mechanics. This figure is from [1].

2.1.1 States

Let us consider a classical event with n possible outcomes. We can describe this event by a probability distribution \wp , corresponding to a vector of n real scalars

$$\wp = (p_1, p_2 \dots p_n); p_i \in \mathbb{R}; 0 \leq p_i \leq 1 \forall i \quad (2.1)$$

with the normalization condition

$$\sum_i |p_i| = 1 \quad (2.2)$$

Quantum mechanics is a theory which naturally emerges if one attempts to replace these probabilities by complex amplitudes, with the condition that the 2-norm, rather than the 1-norm, is conserved.

$$|\psi\rangle = (a_1, a_2 \dots a_n); p_i \in \mathbb{C}; 0 \leq a_i \leq 1 \forall i; \sum_i |a_i|^2 = 1 \quad (2.3)$$

The state of the system is completely encoded in the state vector $|\psi\rangle$, which is defined on the complex Hilber space, \mathcal{H} . Any spot in \mathcal{H} corresponds to a physical state, and two vectors represent the same state iff one is a multiple of the other. This allows construction of superposition states

$$|\psi\rangle = a_1 |\psi_1\rangle + a_2 |\psi_2\rangle \quad (2.4)$$

The Hilbert space has an inner product $\langle \phi | \psi \rangle$, which associates each pair of vectors $|\psi\rangle, |\phi\rangle$ with a complex number, and is positive, linear, and skew symmetric

$$\langle \phi | \psi \rangle \geq 0; \langle \phi | (a |\psi_1\rangle + b |\psi_2\rangle) \rangle = a \langle \phi | \psi_1 \rangle + b \langle \phi | \psi_2 \rangle; \langle \phi | \psi \rangle = \langle \psi | \phi \rangle^* \quad (2.5)$$

Normalization 2.3 can then be re-expressed as $\langle \psi | \psi \rangle = 1$.

In order to describe a composite system of two or more objects, Hilbert spaces are joined by means of the tensor product

$$\mathcal{H}_{AB} = \mathcal{H}_A \otimes \mathcal{H}_B; |\Psi_{AB}\rangle = |\psi_A\rangle \otimes |\psi_B\rangle \quad (2.6)$$

We will normally use two-state system with Hilbert space dimension 2 [2].

2.1.2 Measurements

An observable can be any property of a physical system which can in principle be measured. Observables in quantum mechanics are described by Hermitian operators \hat{A} defined on \mathcal{H} , which map states to states:

$$\hat{A} : |\psi\rangle \rightarrow |\hat{A}\psi\rangle = \hat{A} |\psi\rangle \quad (2.7)$$

Any observable has a spectral decomposition because is Hermitian.

$$\hat{A} = \sum_i \lambda_i \hat{\Pi}_{\lambda_i} \quad (2.8)$$

where λ_i are the eigenvalues. Here, $\hat{\Pi}_{\lambda_i}$ are orthonormal projectors on \mathcal{H} . If λ_i is non-degenerate, then

$$\hat{\Pi}_{\lambda_i} = |\lambda_i\rangle \langle \lambda_i| \quad (2.9)$$

Obviously we will chose $\{|\lambda_i\rangle\}$ such that form an orthonormal basis for \mathcal{H} .

When the observable \hat{A} is experimentally measured, the outcome is always an eigenvalue of \hat{A} . The outcome of any given measurement is in general probabilistic, returning λ_i with probability

$$p(\lambda_i) = \langle \psi | \hat{\Pi}_{\lambda_i} | \psi \rangle \quad (2.10)$$

When we measure the wave function is projected into an eigensatate of \hat{A} corresponding to the measured eigenvalue λ_i . This is called the collapse of the wavefunction. This means that while the system is not measured the state is not defined. This does not mean that is hidden and we can not know which is it. This simply means that the state is uncertain. However when we measure the state, the state will collapse in a particular value and remind there [2].

$$|\psi\rangle \rightsquigarrow \frac{\hat{\Pi}_{\lambda_i} |\psi\rangle}{\sqrt{\langle \psi | \hat{\Pi}_{\lambda_i} | \psi \rangle}} = |\lambda_i\rangle \quad (2.11)$$

2.1.3 Time evolution

As Newton second law of dynamics the quantum systems evolve with time. They follow Schrödinger equation

$$i\hbar \frac{\partial}{\partial t} |\psi\rangle = \hat{H} |\psi\rangle \quad (2.12)$$

Where \hat{H} is the Hamiltonian of the system.

Time-evolution of a closed quantum system can always be described by a unitary operator. In the Schrödinger picture of quantum mechanics, we say that \hat{U} evolves an input state $|\psi\rangle_{in}$ to an output state $|\psi\rangle_{out}$, as

$$|\psi\rangle_{out} = |\psi(t)\rangle = \hat{U} |\psi\rangle_{in} = \hat{U} |\psi(0)\rangle \quad (2.13)$$

[2]

2.1.4 Heisenberg's uncertainty principle

This is probably one of the most weird things about quantum mechanics. Given two observables \hat{C}, \hat{D} we can derive the statistical standard deviation $\Delta(\hat{C}), \Delta(\hat{D})$ for a given unknown state $|\psi\rangle$.

$$\Delta(\hat{C}) \Delta(\hat{D}) \geq \frac{|\langle \psi | [\hat{C}, \hat{D}] | \psi \rangle|}{2} \quad (2.14)$$

For two canonical variables such as position and momentum the expression yields to

$$\Delta(\hat{X}) \Delta(\hat{P}) \geq \frac{\hbar}{2}$$

(2.15)

This means that there is no way to now exactly the position and the momentum at the same time. If we, for example, know the exact position then the momentum could be any value [2].

2.1.5 Qubits

The classical information is encoded with the bit, $b \in \{0, 1\}$. The quantum analogue is the qubit. A qubit is a two-level quantum system. The qubit is a combination of two states $|0\rangle, |1\rangle$ which form a basis for \mathcal{H} .

$$|\psi\rangle = \cos\frac{\theta}{2} |0\rangle + e^{i\phi} \sin\frac{\theta}{2} |1\rangle \quad (2.16)$$

The natural representation for \mathcal{H} is the Bloch sphere. There six states which can be represented on the Bloch sphere as a basis.

$$\begin{aligned} |0\rangle &\equiv [1, 0]^t, |+\rangle \equiv \frac{1}{\sqrt{2}}(|0\rangle + |1\rangle), |+\iota\rangle \equiv \frac{1}{\sqrt{2}}(|0\rangle + \iota |1\rangle) \\ |1\rangle &\equiv [0, 1]^t, |-\rangle \equiv \frac{1}{\sqrt{2}}(|0\rangle - |1\rangle), |-\iota\rangle \equiv \frac{1}{\sqrt{2}}(|0\rangle - \iota |1\rangle) \end{aligned} \quad (2.17)$$

Which are eigensates of the Pauli matrices $\hat{\sigma}_z, \hat{\sigma}_x, \hat{\sigma}_y$ respectively [2].

2.2 Linear optics quantum computing

In the last section we have seen the basic concepts of quantum mechanics. The aim of the last section was not to give a detailed picture of quantum mechanics but a brief idea about the key points. In this section we are going to do quantum computation by using integrated photonics. We will start with the basic way to encode qubits. Then we will introduce the different linear nano-devices that are part of a more complex integrated quantum system. Finally we will explain the main ideas to implement quantum computation on chip.

2.2.1 Path-Encoded Qubits

As we have seen the qubit is the basic information unit in quantum mechanics. If we have more than one qubit we can represent the state of each as a strings of zeros and ones: $|111\rangle$ represents three qubits, each in the 1 state, for example.

A single qubit can be represented as a point on the surface of the Bloch sphere given by the polar angle θ and the azimuthal angle ϕ (2.2).

In integrated photonics qubits are encoded in the path degree of freedom. This qubits are know as dual-rail qubits. But we are going to refer to them simply as path qubits. A path qubit is a photon spread between two spatial modes. This will be the modes of single-mode waveguides. Then a path qubit lives within a pair of waveguides. We can manipulate such qubits with rotations around the Bloch sphere. A rotation \hat{R}_z can be performed using a phase shifter in one of the waveguides. And a rotation \hat{R}_y can be performed using a phase shifter between two beam splitters, in other words a Mach-Zehnder interferometer (MZI) [3].

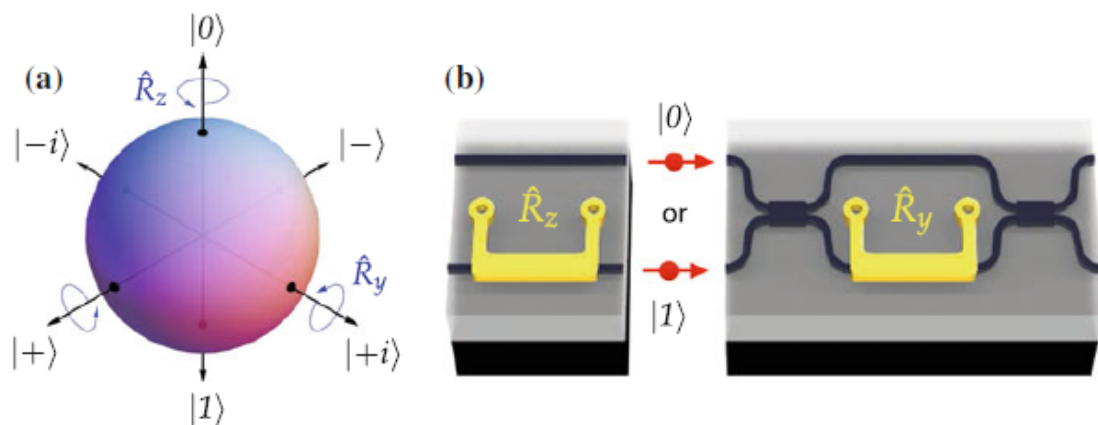


FIGURE 2.2: a) Bloch sphere representation of a qubit. b) The qubit occupies one of the two waveguide modes. The gold part represents a heater which allows to create a phase shift between waveguides c) The two x shapes represent beam splitters and all the structure is a MZI [3].

This figure is on

Using three rotations we can transform every state $|\phi\rangle$ to an other arbitrary state $|\psi\rangle$.

$$|\psi\rangle = \hat{R}_z(\theta_2)\hat{R}_y(\theta_1)\hat{R}_z(\theta_0)|\phi\rangle \quad (2.18)$$

This allows us to be able to prepare any qubit state by using a phase shifter and a MZI. This also allows us to measure in any base we want. We just need again a phase shifter and a MZI. We can see a arbitrary state preparation and arbitrary base measurement on FIGURE 2.3.

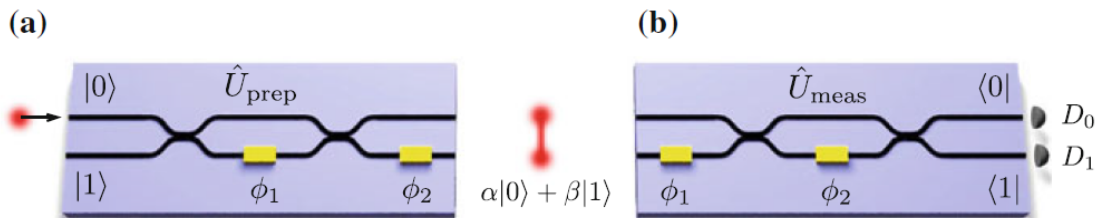


FIGURE 2.3: a) General state preparation. b) General base measurement [2].

This figure is on

2.2.2 Unitary operations transformation

In order to do linear optics quantum computing three main elements are required. We will need **single photon sources** to generate single photons that will propagate through waveguides. Then we need **reconfigurable MZI** to manipulate the photon states. After that we will need **single photon detectors** to detect the photons. As we have already seen, we need a MZI and a phase shifter to implement an arbitrary unitary operation on two modes ($\hat{U} \in SU(2)$), in other words, to generate a general single qubit state. How can we generalize this to systems with more than two modes? Which operations can we implement on m modes, using only linear-optical elements?

As shown by Reck and Zeilinger [5], any $m \times n$ unitary operator \hat{U} corresponds to a linear-optical circuit on m modes, constructed from beamsplitters and phase-shifters only. That is, any \hat{U} has a decomposition as a product

$$\hat{U} = \hat{U}_T \hat{U}_{T-1} \dots \hat{U}_1 \quad (2.19)$$

where each \hat{U}_T acts nontrivially on at most two modes and does not affect the remaining $m-2$ modes. A simple proof has been given by Aaronson and Arkhipov [6]. Given any \hat{U} target the task is to perform the 2.19 decomposition. Different people have found different ways to do this decomposition the first one was Reck on 1994 [5], this last march a new configuration of beam splitters and phase shifters has been discovered and uses half of the physical foot print of the Reck design and is significantly more robust to optical losses [6].

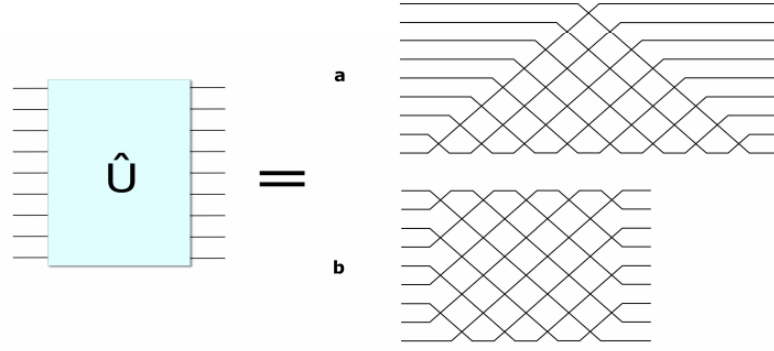


FIGURE 2.4: A universal N-mode multipoint interferometer a) the one proposed by Reck or b) the one that Aaronson and company [6] demonstrate. This figure appears on [6]

We have seen that we can implement any unitary matrix, then does that mean that we can build a universal gate-set for a quantum computer using only beamsplitters and phase-shifters? The answer is no. We need to build at least an other quantum gate to perform quantum computation. This gate is called the control not gate or CNOT. With a CNOT gate and single qubits unitary transformations we can do any quantum algorithm. But why can we not create a CNOT gate using the decomposition technique that we have seen before? The answer is that a CNOT gate has a non-linearity. We will study the CNOT gate on section 2.4.

2.3 Puzzle pieces

In this section we will describe the main devices for quantum integrated photonics and how they work separately.

2.3.1 Quantum beam splitter

We want to study how two photons interfere when they enter in a beam splitter. First, we consider a beam splitter parameterized in the following way

$$S^T = \begin{bmatrix} \sqrt{R} & i\sqrt{T} \\ i\sqrt{T} & \sqrt{R} \end{bmatrix} \quad (2.20)$$

we label the two input spatial modes as a and b, and the two output spatial modes as c and d. Imagine that each photon arrives at a different time for example t_1 mode a and t_1 mode b. Then they are fully distinguishable. The input state will be

$$|\Psi_{in}\rangle = |11\rangle = a_{t_1}^\dagger b_{t_1}^\dagger |00\rangle \quad (2.21)$$

where the operators $a_{t_1}^\dagger, b_{t_2}^\dagger$ are the creation operators for the modes a and b respectively when applied to the vacuum state. with their output state given by

$$\begin{aligned} |\Psi_{out}\rangle &= (\sqrt{R}c_{t_1}^\dagger + i\sqrt{T}d_{t_1}^\dagger)(\sqrt{R}d_{t_2}^\dagger + i\sqrt{T}c_{t_2}^\dagger) |0000\rangle \\ &= [i\sqrt{RT}(c_{t_1}^\dagger c_{t_2}^\dagger + d_{t_1}^\dagger d_{t_2}^\dagger) + Rc_{t_1}^\dagger d_{t_2}^\dagger - Tc_{t_2}^\dagger c_{t_1}^\dagger] |0000\rangle \\ &= i\sqrt{RT}(|1100\rangle + |0011\rangle) + R|1001\rangle - T|0110\rangle \end{aligned} \quad (2.22)$$

where the Fock basis order is $|0_{ct_1}0_{ct_2}0_{dt_1}0_{dt_2}\rangle$. Then for a balanced beam splitter the coincidence between modes c and d is $P_{dist} = \frac{1}{2}$.

Let us say the photons arrive at the same time and then are indistinguishable.

$$|\Psi_{in}\rangle = |11\rangle = a^\dagger b^\dagger |00\rangle \quad (2.23)$$

and then the output will be

$$\begin{aligned} |\Psi_{out}\rangle &= (\sqrt{R}c^\dagger + i\sqrt{T}d^\dagger)(\sqrt{R}d^\dagger + i\sqrt{T}c^\dagger) |vac\rangle \\ &= [i\sqrt{RT}(c^{\dagger 2} + d^{\dagger 2} + c^\dagger d^\dagger [R-T])] |vac\rangle \\ &= i\sqrt{2RT}(|20\rangle_{cd} + |02\rangle_{cd}) + (R - T) |11\rangle_{cd} \end{aligned} \quad (2.24)$$

For a balanced beam splitter $P_{dist} = (R - T)^2 = 0$. This destructively interference is a quantum sign. This forces the two photons to exit the beam splitter together form the same spatial output mode. This effect is called Hong Ou Mandel effect [3].

2.3.2 Phase shifter and MZI

The phase shifter is key to implement path-encoded photonic qubits. A phase shifter leads to the MZI. For a MZI the transfer matrix is

$$U_{MZI} = ie^{-\frac{\phi}{2}} \begin{bmatrix} -\sin(\frac{\phi}{2}) & \cos(\frac{\phi}{2}) \\ \cos(\frac{\phi}{2}) & \sin(\frac{\phi}{2}) \end{bmatrix} \quad (2.25)$$

Let us consider two-photon input state, $|11\rangle$.

$$\begin{aligned} &= |11\rangle = a^\dagger b^\dagger |00\rangle \\ \rightarrow & \left[\frac{\sin(\phi)}{2} (d^{\dagger 2} - c^{\dagger 2}) + \cos(\phi) c^\dagger d^\dagger \right] |vac\rangle \\ &= \frac{\sin(\phi)}{\sqrt{2}} (|02\rangle - |20\rangle) + \cos(\phi) |11\rangle \end{aligned} \quad (2.26)$$

Then if we measure coincidences the probability change with ϕ as $p(|11\rangle) = \cos^2(\phi)$ [3].

2.3.3 Single photon source

introduction

In order to do quantum integrated photonics we would like a single photon source of on demand photons. The most well known way to generate photon pairs is the parametric down conversion which uses the nonlinear coefficient χ^2 . However this coefficient is too small in silicon. Yet silicon benefits from a large $\chi^{(3)}$ third-order non-linearity which enables spontaneous four-wave mixing or SFWM. This is an elastic process by which two photons from a bright laser beam are converted into two photons at different frequencies, which we label as signal (with average wave number k_s , and angular frequency ω_s) and idler (width wave number k_i , and angular frequency ω_i). This photon-pair source can then be used as a heralded single-photon source (by measuring one photon and thus heralding its partner) which, in combination with fast switches enables the generation of single photons on-demand.

Theory of SFWM Sources

For a given nonlinear interaction medium supporting a single spatial mode a , the process is described by the following Hamiltonian

$$\hat{H} = \hat{H}_L + \hat{H}_{NL} \quad (2.27)$$

where

$$\hat{H}_L = \int dk \hbar \omega_k a_k^\dagger a_k \quad (2.28)$$

in the vacuum Hamiltonian. And the nonlinear interaction is given by the SFWM Hamiltonian

$$\hat{H}_{NL} = \int dk_1 dk_2 dk_3 dk_4 S(k_1, k_2, k_3, k_4) a_{k_1}^\dagger a_{k_2}^\dagger a_{k_3} a_{k_4} + H.c. \quad (2.29)$$

where H.c. stands for Hermitian conjugate, and S captures the interaction between the different modes of the structure we are interested in (i.e., the input pump modes and the output single-photon modes). We are not going to derive the output state from the Hamiltonian but we are going to give the expression to first order [1].

$$|\Psi_{out}\rangle = \left[1 + \frac{i\beta}{\sqrt{2}} \int dk_1 dk_2 \Phi_{II}(k_1, k_2) a_{k_1}^\dagger a_{k_2}^\dagger \right] |vac\rangle \quad (2.30)$$

$$\Phi_{II}(k_1, k_2) = \frac{2\sqrt{2}\pi\alpha^2}{\hbar\beta} \int dk_3 dk_4 \Phi_p(k_3) \Phi(k_4) S(k_1, k_2, k_3, k_4) \delta(\omega_1 + \omega_2 - \omega_3 - \omega_4) \quad (2.31)$$

where Φ_p is the normalized pump spectral distribution, α is the amplitude of the pump, and β is defined such that

$$\int | \Phi_{II}(k_1, k_2) |^2 dk_1 dk_2 = 1 \quad (2.32)$$

Φ_{II} describes the shape of the joint spectral probability amplitude distribution between the signal and idler photons. It encapsulates all the contributions from the pump spectrum, the waveguide dispersion, energy conservation, and any spectral structure due to the system considered. β reflects the efficiency of the source [3].

2.3.4 Single photon detector

Introduction

In the past few decades new photonics applications have been discovered. A lot of applications increasingly need single photon detection. For example single photon detection is needed for ultra-high resolution single-molecule fluorescence microscopy [8] high-sensitivity optical communications, quantum experiments and quantum key distribution among others. Therefore a new device called single-photon detector has been invented. The ideal single-photon detector absorbs a photon and produces an electrical signal that can be captured. This process always happens and does not depend on photon's frequency, shape or polarization. In reality, the ideal single-photon detector does not exist. Different types of detectors have been used for different frequency regions. For the visible spectrum, the best approach is the semiconductor based sensors which basically use an avalanche diode effect. These sensors achieve a maximum efficiency of

76% at 700nm FIGURE 3.8. However they are not useful at telecom IR wavelengths. This problem has been solved with a completely different sensor design. Just fourteen years ago a new superconducting device concept was created by Alex D. Semenov [10] and demonstrated by Gol'tsman et al, based on a niobium nitride nanowire [7]. This type of device, known as the superconducting nanowire single-photon detector (SNPD), is single-photon sensitive at visible and infrared wavelengths, with recovery times and timing precision order of magnitude faster than existing single-photon detectors based on superconducting materials. In addition, this detector operates at the boiling point of liquid helium (4.2K).

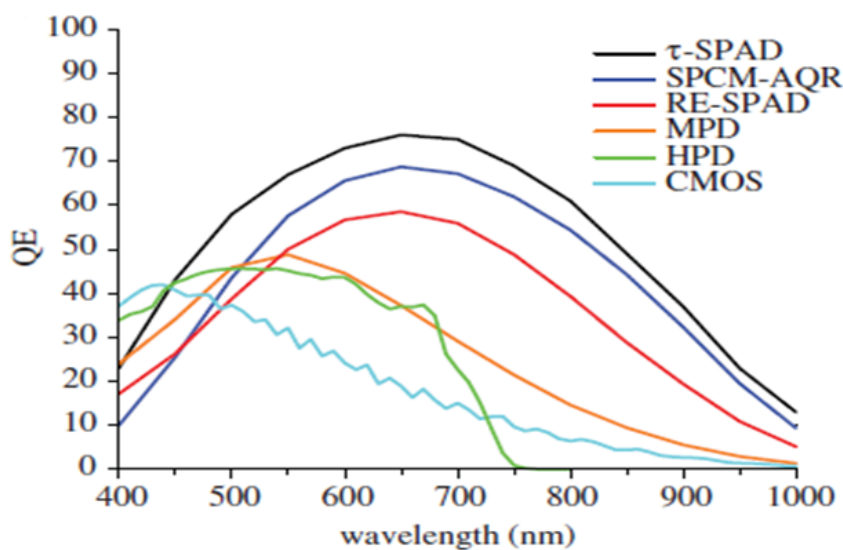


FIGURE 2.5: Quantum efficiencies (QEs) of different types of silicon detectors. Curves were provided by the manufacturers [8].

Application details

Firstly, I am going to introduce different parameters which involve single-photon detectors and more specifically SNPD. The system detection efficiency is defined as the probability of detecting a photon. This probability depends on the probability of absorbing a photon, the registering probability, which is the probability that the sensor generates an output electrical signal after photon absorption, and finally the coupling probability, which is the probability that the photon arrives correctly to the sensor. If we consider a perfect coupling then we have what is called Quantum efficiency (QE). The timing latency gives an idea of about how long it takes from the photon being absorbed until the electrical pulse can be measured. This delay between the absorption and the output signal is not constant and in general it can change a little every measurement. The jitter measures the standard deviation in the detection time of the detector. The dark counts are counts a detector registers when no light from our source is incident on it. The after pulsing gives an idea about correlated false counts that happened some time after the initial detection event. The recovery time is how long it takes before a detector is ready to detect the next photon. In the following FIGURE 2.6 we can see this properties for the device reported in [12; 13].

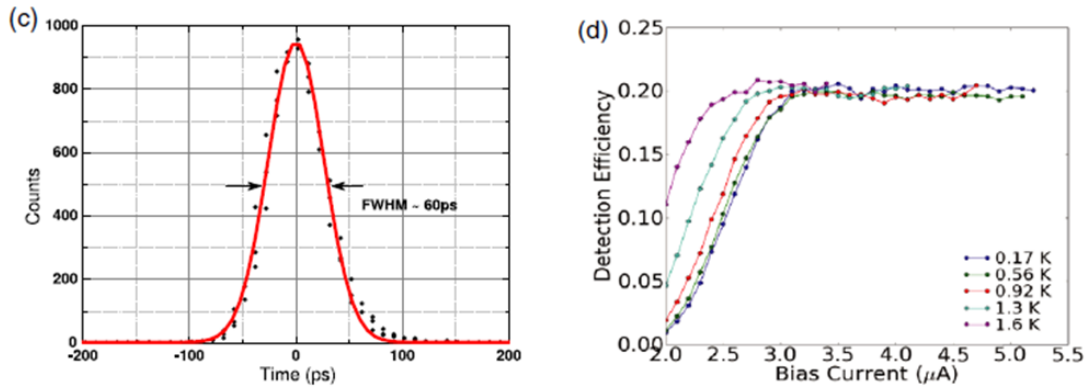


FIGURE 2.6: The characteristics of SNSPDs (c) the instrument response function of a NbTiN SNSPD measured using a femtosecond laser and TCSPC card at $\lambda = 1550$ nm. The 1σ of 60 ps FWHM is quoted as the jitter of the device in [6], (d) a SNSPD fabricated in a low energy gap superconductor, ($\lambda = 1550$ nm) occurs at higher bias currents [13; 9].

The mechanism of single photon detection by thin superconducting films biased close to the critical current of the film consists in the formation of the hot spot in the place of photon absorption resulting in voltage pulse generation, which can be easily measured. SNSPD consists of a superconducting stripe of a submicrometer width (comparable with the hotspot size) whose thickness is less than the electron thermalization length. The device is maintained at a temperature much lower than that of superconducting transition T_c and biased close to the device critical current I_c . The photoresponse mechanism is presented in FIGURE 2.7. The collective action of the hotspot formation and I_b redistribution results in the appearance of the macroscopic resistive barrier across the SNPD stripe [1]. As is illustrated in Fig. 3, after the localized hotspot is created (FIGURE 2.7(a)), it then grows as quasiparticle diffuse out of the hotspot core. Simultaneously, the biasing supercurrent I_b is expelled from the resistive hotspot volume and concentrated in the “sidewalks” near the edges of the film (FIGURE 2.7 (b)). Thus, I_b exceeds the critical value outside the hotspot, and phase-slip centres are created in quasi-one-dimensional sidewalks (FIGURE 2.7(c)). As a result, the superconductivity is destroyed, and a resistive barrier is formatted across the entire cross-section of the stripe (FIGURE 2.7(d)). The resistive barrier gives rise to a voltage signal with the amplitude proportional to I_b . After its growth phase, the hotspot decreases due to the relaxation and out-diffusion of quasiparticles. Thus, after the quasiparticle relaxation time the hotspot in the stripe collapses, superconductivity is restored, and the detector is ready to register another photon .

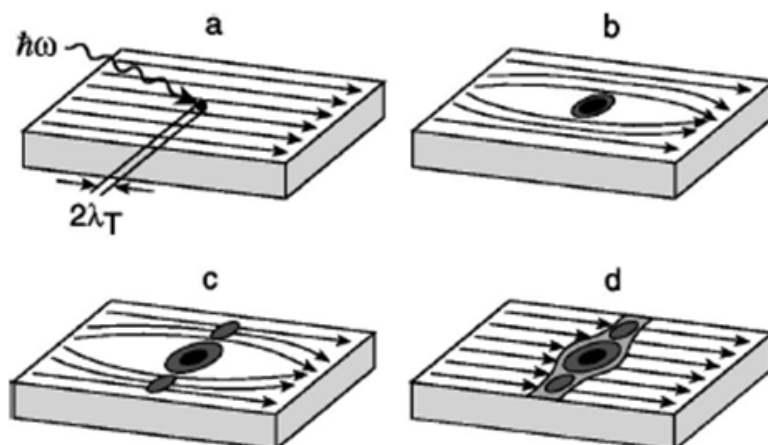


FIGURE 2.7: Schematics of the supercurrent-assisted hotspot formation mechanism in an ultrathin and narrow superconducting strip, kept at temperature far below T_c are shown. The arrows indicate direction of the supercurrent flow [7].

State of the art

The best SNSPDs are currently made at NIST, Boulder Colorado. In 2013 they achieved a 93% efficiency, low dark count rate ($<1\text{c.p.s.}$), low timing jitter ($<100\text{ps}$) and short reset time ($<100\text{ns}$) at $\lambda = 1520 - 1610\text{ nm}$ [11].

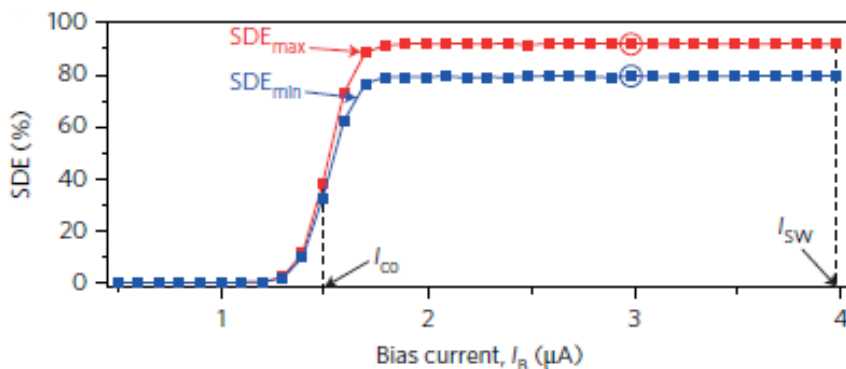


FIGURE 2.8: Bias current dependence SDE or QE for two different polarizations of light at $\lambda = 1500\text{ nm}$ [11].

2.4 Quantum algorithms applied to integrated optics

In this chapter we have seen the foundations for quantum mechanics, how qubits can be encoded and how to perform any unitary operation in an arbitrary number of qubits. Those things are really interesting but there are not enough to implement quantum algorithms on integrated photonics. Why? We would think that we can do computation

just applying unitary transformations on our qubits. But in reality the really computation relies on non linear operations.

Is is well known that we can build any logic classical gate by using only NAND gates. In quantum computation is well-known [18] that a universal set of 1-qubit gates, together with any entangling 2-qubit gate (such as the CNOT gate), composes a universal set for n-qubit operations. That means that with CNOT gates and unitary operations we can implement any quantum algorithm.

But then how can we build a CNOT gate on integrated optics? In literature we found three main different approaches to do it [19; 20; 21]. All three have in common the use of measurement as a non linearity and those three approaches are from the year 2001. The two first [19; 20] are a general way to implement quantum gates and the third one [21] is a specific way to implement a CNOT gate on integrated photonics using post-selection and linear optics. We will see in more detail [19; 21] because [19; 20] are really similar.

Before let us understand what a CNOT gate is and what it does.

2.4.1 The CNOT gate

A CNOT gate is a two qubit gate. The first qubit is called control qubit and the second qubit is called target qubit. The output at the control qubit remains the same. The output at the target qubit is going to be the same if the state on the control qubit is $|0\rangle$. But if the control qubit state is $|1\rangle$ then the state on target qubit will flip. The representation for a CNOT gate in quantum computation notation is the following (FIGURE 2.9).

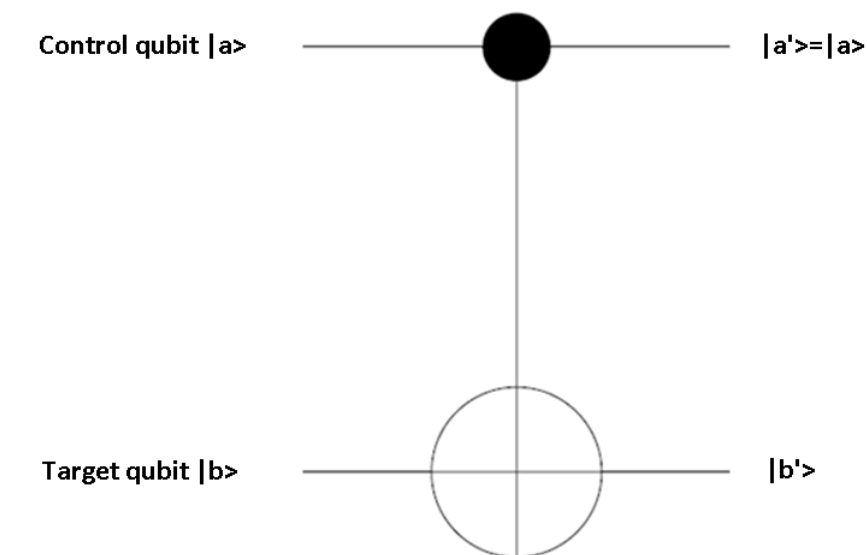


FIGURE 2.9: CNOT quantum gate scheme

2.4.2 Measured based quantum computation

One-way quantum computation, measurement based quantum computation or MBQC is a way to think about quantum computing. MBQC relies on the nonlinearity of measurements to perform quantum operations. The idea is to start with a cluster of entangled qubits. Then by measuring those qubits with different bases we will perform quantum operations. It sounds complicated but is not. We will see how to build the CNOT. First we need to define a few things:

$$\begin{aligned}
 & N_i = |+\rangle \\
 E_{ij} = & \begin{pmatrix} 1 & 0 & 0 & 0 & 0 & 0 & 0 & 0 & \dots & 0 \\ 0 & 1 & 0 & 0 & 0 & 0 & 0 & 0 & \dots & 0 \\ 0 & 0 & \ddots & 0 & 0 & 0 & 0 & 0 & \dots & 0 \\ 0 & 0 & 0 & 1 & 0 & 0 & 0 & 0 & \dots & 0 \\ 0 & 0 & 0 & 0 & -1 & 0 & 0 & 0 & \dots & 0 \\ 0 & 0 & 0 & 0 & 0 & 1 & 0 & 0 & \dots & 0 \\ \vdots & 0 & 0 & 0 & 0 & 0 & 0 & \ddots & \dots & 0 \\ 0 & 0 & 0 & 0 & 0 & 0 & 0 & 0 & 1 & 0 \\ 0 & 0 & 0 & 0 & 0 & 0 & 0 & 0 & 0 & 1 \end{pmatrix} \quad (2.33) \\
 & M_i^\alpha = \langle \pm_\alpha | \rightarrow s_i = 0, 1 \\
 & X_i^s = \begin{pmatrix} 0 & 1 \\ 1 & 0 \end{pmatrix}^s, Z_i^s = \begin{pmatrix} 1 & 0 \\ 0 & -1 \end{pmatrix}^s
 \end{aligned}$$

We start with n qubits. N_i sets qubit i to $|+\rangle = \frac{1}{\sqrt{2}}(|0\rangle + |1\rangle)$ state. The operation E_{ij} is a controlled phase gate CZ and is defined by

$$E_{ij}|i\rangle|j\rangle = (-1)^{ij}|i\rangle|j\rangle \quad (2.34)$$

So it introduces a π phase shift if both qubits i and j are in state $|1\rangle$. M_i^α measures qubit i in the base $\langle \pm_\alpha |$ the output of this measurement is coded on s_i which will be 0 if we measured $\langle +_\alpha |$ and 1 if we measured $\langle -_\alpha |$. Finally X_i^s, Z_i^s are two of the basic Pauli operators. X_i flips the state on qubit i. Z_i flips the sign on qubit i. Those will act to the qubit i if the measurement s is 1 too.

Once we defined the basic operations we can start building a CNOT gate. In order to do that we will need 4 qubits. Qubit 1 and 2 will be the control and target qubits respectively. Qubits 3 and 4 will start in the $\langle + |$ state. Then we will apply CZ operations between cubits 1-3,2-3,3-4. After that we will measure qubits 2 and 3 using $\langle \pm |$ base. Finally we will apply corrections on qubit 4 depending on the measurement outputs. Then the target qubit output is going to be on qubit 4 []. We can see an symbolic representation of that on FIGURE 2.10.

$$CNOT = X_4^{s_3} Z_4^{s_2} Z_1^{s_2} M_3^0 M_2^0 E_{13} E_{23} E_{34} |a\rangle |b\rangle N_3 N_4 \quad (2.35)$$

If we do the math on (2.35) is straightforward to see that is doing a CNOT operation.

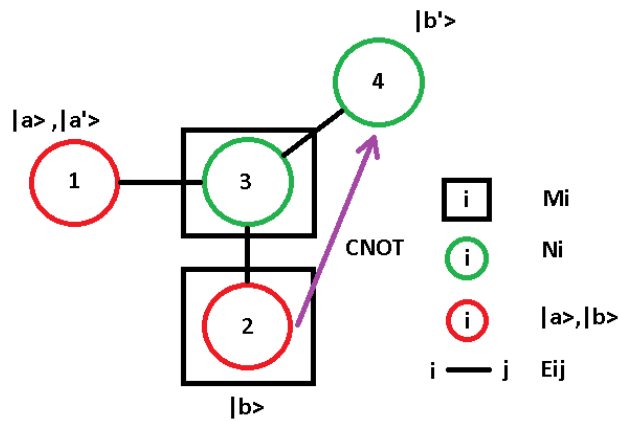


FIGURE 2.10: MBQC CNOT quantum gate scheme

It is not clear yet how implement MBQC in integrated photonics. Yet is clear that we will need to feedforward fast signals and perform operations depending on those signals. The other problem es to implement a CZ gate, that is a non-linear gate. Knill,Laflamme and Milburn or KLM proposed an alternative way that does not need CZ gates [20; 22] but still using feedforward as the MBQC that we have already seen.

2.4.3 Linear optical controlled-NOT gate

In this subsection we will give an over view of T.C. Ralph design. For a detailed explanation see [2; 21]. T.C. Ralph inspired the design on KLM paper [20; 22] but does not use feedforward it uses postselection instead. This design is not scalable meaning that we can demonstrate only one CNOT gate but not more. This is due to the fact that the success probability of the gate is $\frac{1}{9}$ That means that assuming that we can simply cascade n CNOT gates with 100% efficiency (which is not true a plus does it make sense) then the success probability will be $\frac{1}{9^n}$. In FIGURE 2.11 we can see the schematics

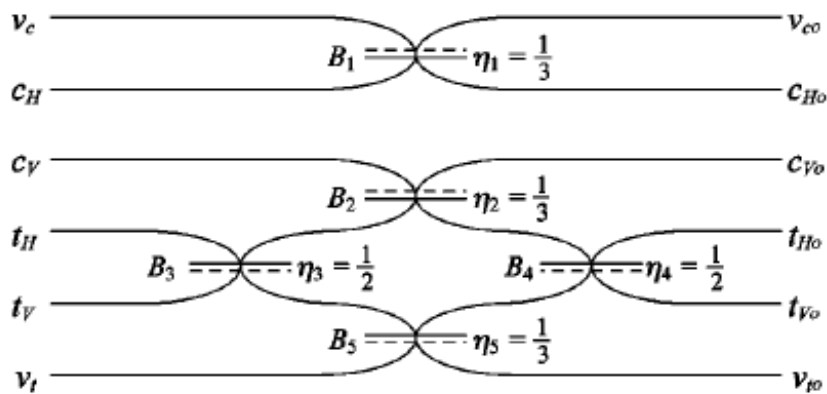


FIGURE 2.11: Schematic of the coincidence controlled-NOT gate. c corresponds to control, t corresponds to target, and v are unoccupied [?]ralph). H and V refers to vertical and horizontal polarizations. But those photons are path encodets, so for us H is going to be 0 and V is going to be 1.

We are not going to do the maths but is straightforward [?]ralph) to prove that the schematic acts as a CNOT gate if we only take into account the cases that make sense. Ergo we have to measure two photons coincidences but the one photon has to be in a control mode and the other one in a target mode.

Chapter 3

Designing a broadband beam splitter

The present is theirs; the future, for which I really worked, is mine.

Nikola Tesla

The aim of this chapter is to describe the simulation and design of a new type of coupler that personally developed the last six month at Nanophotonics lab. In this chapter we are going to explore the different kinds of beam splitters in the literature. In order to do that first, we are going to introduce the slab waveguide to understand the basic concepts. Then we are going to extrapolate to a three dimensional waveguide. We use waveguides to confine light inside the chip. After understanding the waveguides we are going to introduce coupled mode theory, supermode picture and adiabatic theory to be able to describe property the different type of couplers. Once we understand the theory we are going to the results of simulating lowloss couplers from literature using codes developed in PLAB. Finally, we are going to describe the operation of how we invented a new type of coupler conceived and developed during this project.

3.1 Slab waveguide

Firstly we want to introduce the concept of optical guidance. Imagine a long square metallic pipe made of metal with air inside. If an electromagnetic wave gets into the pipe it will hit the walls and reflect as in a mirror and hit an other wall and reflect again and so on. Then we can say that the square metallic pipe is guiding the electromagnetic wave. However we are working with optical frequencies and metal generates high losses at these frequencies. We can use the same idea to guide optical frequencies.

The simplest optical waveguide is the dielectric slab. Is one of the few structures which can be solved analytically. Understanding the slab waveguide is really useful to understand three dimensional waveguides.

The major phenomenon that makes slab waveguides working is the total internal reflection. This happens in the interface between two dielectrics if the indecent angle is small enough. From geometrical optics we know that a ray of light will follow the Snell's law while crossing interface separating two different dielectrics.

$$n_1 \sin(\Theta_1) = n_3 \sin(\Theta_3) \quad (3.1)$$

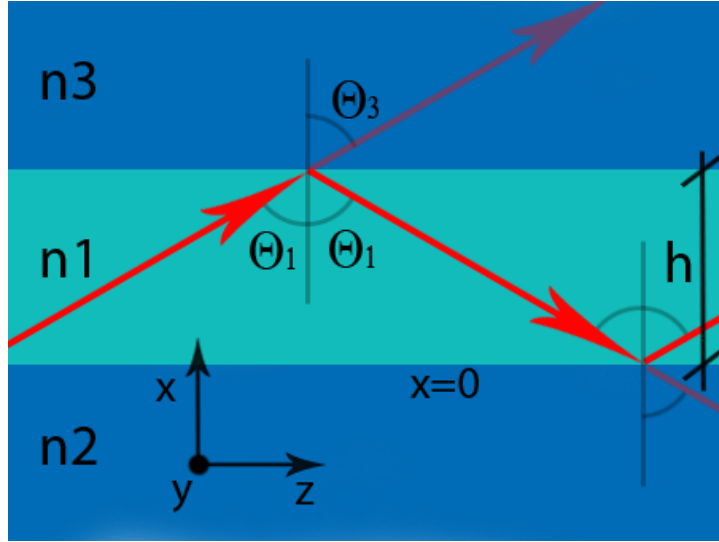


FIGURE 3.1: In this figure we can see the slab waveguide geometry. It consist in three layers of different dielectrics which their respective refractive indexes. Red arrows represent the rays traveling through the structure.

We define the critical angle Θ_c the angle just before internal reflection. So the condition for the critical angle is $\Theta_3 = \pi/2$.

$$\Theta_c = \text{asin}\left(\frac{n_3}{n_1}\right) \quad (3.2)$$

Then all the waves with incident angles $\Theta_1 > \Theta_c$ will be guided due to internal reflection.

To understand the shape of the electric fields that propagate inside the structure we can find the modal solutions. The modes are defined as the eigenvalues of the structure when the Maxwell equations are applied. First we will show the general form of Maxwell equations.

$$\begin{aligned} \nabla \times \mathbf{H} &= \epsilon_o n^2 \frac{\partial \mathbf{E}}{\partial t} \\ \nabla \times \mathbf{E} &= -\mu \frac{\partial \mathbf{H}}{\partial t} \end{aligned} \quad (3.3)$$

The cross indicates a vector product, \mathbf{H} and \mathbf{E} are the magnetic and electric field vectors, and ϵ_o and μ_o are the dielectric permeability and magnetic permeability of vacuum. Magnetic and conductive materials are not considered. The index of refraction of the medium is designated by n , and t is the time variable.

We simplify the description of the slab waveguide by assuming that there is no variation in y direction, which we express symbolically by the equation

$$\frac{\partial}{\partial y} = 0 \quad (3.4)$$

Those solutions have constant speed and move in z direction. For simplicity and without losing generality we are assuming polarization in y direction. So, that the mode is Transverse Electric, or **TE**. The other polarization: Transverse Magnetic, or **TM** can be solved analogously. Manipulating the general Maxwell equations we find the scalar equation that has to be satisfied for each layer.

$$\nabla^2 E_{yi}(x, z) + n_i^2 k_o^2 E_{yi}(x, z) = 0 \quad (i = 1, 2, 3) \quad (3.5)$$

As it has been mentioned we are going to try the following solution where β is the propagation constant.

$$E_{yi}(x, z) = E_i(x) \exp(-j\beta z) \quad (i = 1, 2, 3) \quad (3.6)$$

And then we will have to solve the following equation to find the possible values of β

$$\frac{d^2 E_i}{dx^2} + [n_i^2 k_o^2 - \beta^2] E_i = 0 \quad (3.7)$$

We are looking for confined fields within the guide. This means standing wave inside the guiding layer and evanescent fields outside. Then we can write this trial solutions.

$$\text{In layer 1: } E_1 = E \cos(\kappa x - \phi)$$

$$\text{In layer 2: } E_2 = E' \exp(\gamma x) \quad (3.8)$$

$$\text{In layer 3: } E_3 = E'' \exp(-\delta(x - h))$$

where the constants κ, γ and δ are given by

$$\begin{aligned} \kappa &= \sqrt{n_1^2 k_o^2 - \beta^2} \\ \gamma &= \sqrt{\beta^2 - n_2^2 k_o^2} \\ \delta &= \sqrt{\beta^2 - n_3^2 k_o^2} \end{aligned} \quad (3.9)$$

The boundary conditions have to be satisfied. This means continuity of $E_i(x)$ and its gradient $\frac{dE_i}{dx}$ at each interface. At $x=0$ we get

$$\begin{aligned} E' &= E \cos(\phi) \\ \gamma E' &= -\kappa E \sin(-\phi) \end{aligned} \quad (3.10)$$

which leads to a closed-form expression for ϕ

$$\tan(\phi) = \frac{\gamma}{\kappa} \quad (3.11)$$

Similarly at $x=h$ we get

$$\begin{aligned} E'' &= E \cos(\kappa h - \phi) \\ -\delta E'' &= -\kappa E \sin(\kappa h - \phi) \end{aligned} \quad (3.12)$$

and therefore:

$$\tan(\kappa h - \phi) = \frac{\delta}{\kappa} \quad (3.13)$$

Then manipulating both expressions we finally get the dispersion relation for the slab wave guide:

$$\tan(\kappa h) = \kappa \frac{\gamma + \delta}{\kappa^2 - \gamma\delta} \quad (3.14)$$

This equation has a discrete set of solutions for β . We can solve this equation numerically and find which are the possible values for β . If we do it for every width we are going to get the dispersion curve.

Every mode has a propagation velocity. From simple optics we know that the phase velocity is simply the speed of light over the refractive index. So we define the effective refractive index of each mode:

$$n_{eff} = \frac{\beta}{k_0} = \frac{\beta\lambda}{2\pi} \quad (3.15)$$

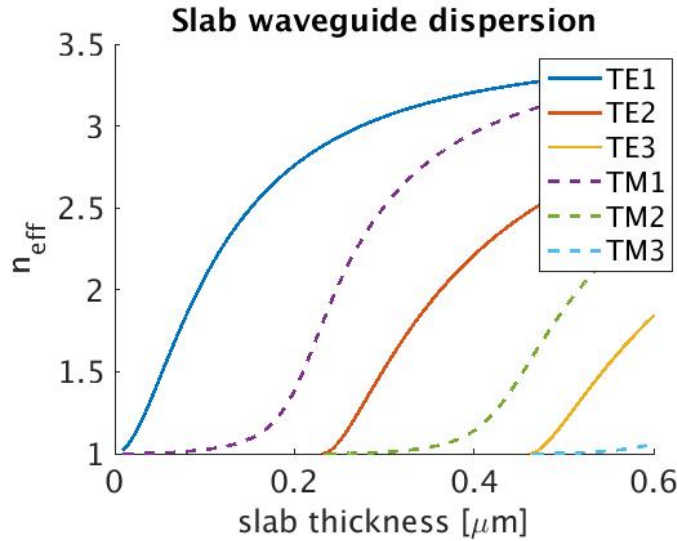


FIGURE 3.2: In this figure we can see how the propagation constant is changing with width for both polarizations. For each width exist a set of possible modes propagating through the dielectric. The Y-axis is in units of n_{eff} . This is directly related to the propagation constant: $n_{eff} = \frac{\beta}{k_0}$. In this structure $n1 = 3.47$ (Si) , $n2 = n3 = 1$ (Air) @1550nm

As we can see, for the indicated refractive index values in FIGURE 3.2 if the slab thickness is less than $0.2\mu m$ we are going to have only one mode in each polarization. The first mode is called fundamental mode. A waveguide that only guides the fundamental mode is called monomode waveguide. In future we will like to have monomode waveguides. It can be prove that the set of modes is complete. Every mode is perpendicular respect to the others. This condition implies that the overlap integral over the volume for the product of the electric field of two modes i and j is the δ_{ij} . They also have a number of nulls depending on the number of modes. For example the fundamental mode does not have any null. The first mode has a null, the second has two and so on [14].

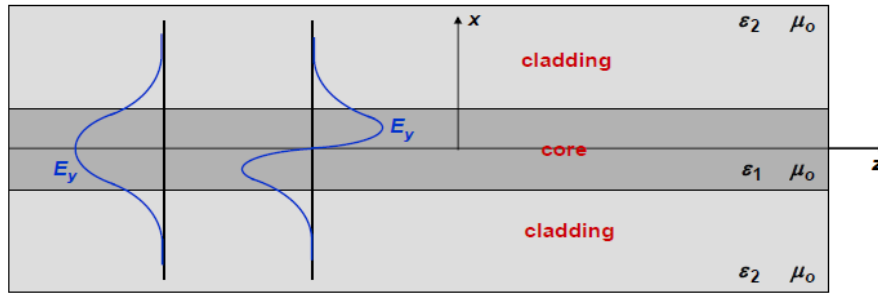


FIGURE 3.3: In this figure we can see the first two TE modes.

3.2 3D waveguides

In the last section we studied the slab waveguide. It is a 2D structure and it could seem useless in a 3D world. However, the slab waveguide is used as a good approximation when one of the dimensions is much higher than the others.

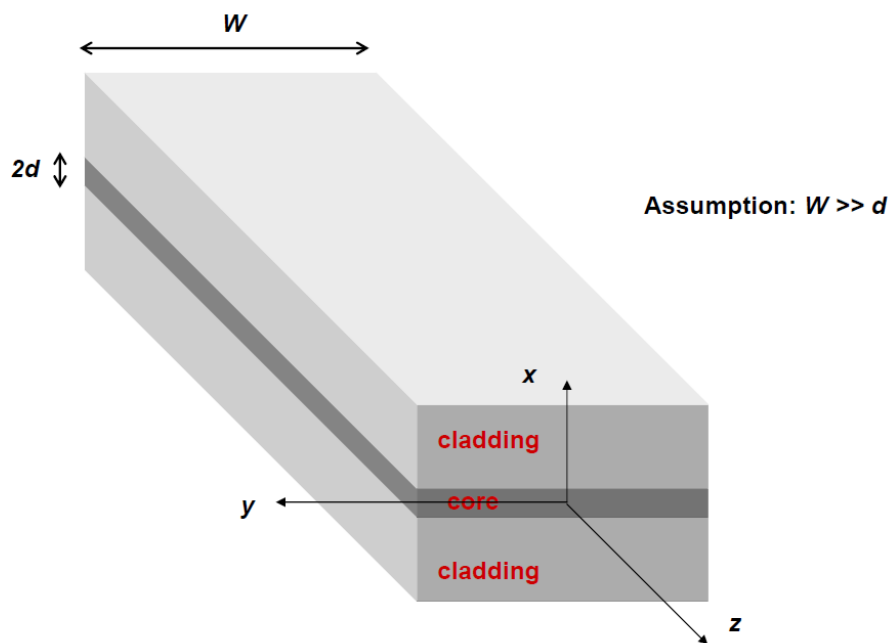


FIGURE 3.4: In this figure we can see the slab waveguide geometry in a three dimensional world.

When the core dimensions have the same order of magnitude in both directions at the cross section then we can not do the slab waveguide approximation. Moreover, we can not find the general expression for the modes.



FIGURE 3.5: We can approximate the modes in x direction as a slab waveguide for the left structure. However we can not compute the y direction modes using the slab waveguide approximation. The right structure is the one we will be dealing with for our designs. It can have air cladding or SiO_2 cladding.

Therefore for now on we are going to use powerful numerical tools to deal with 3D dielectric structures. Most of those codes have been developed by Prof. Miloš Popović during his Ph.D.

The first code we are going to use is the modesolver. This code gets a cross section as an input and computes the modes and propagation constant. It also have a visualization tool which allows to visualize and sort the modes.

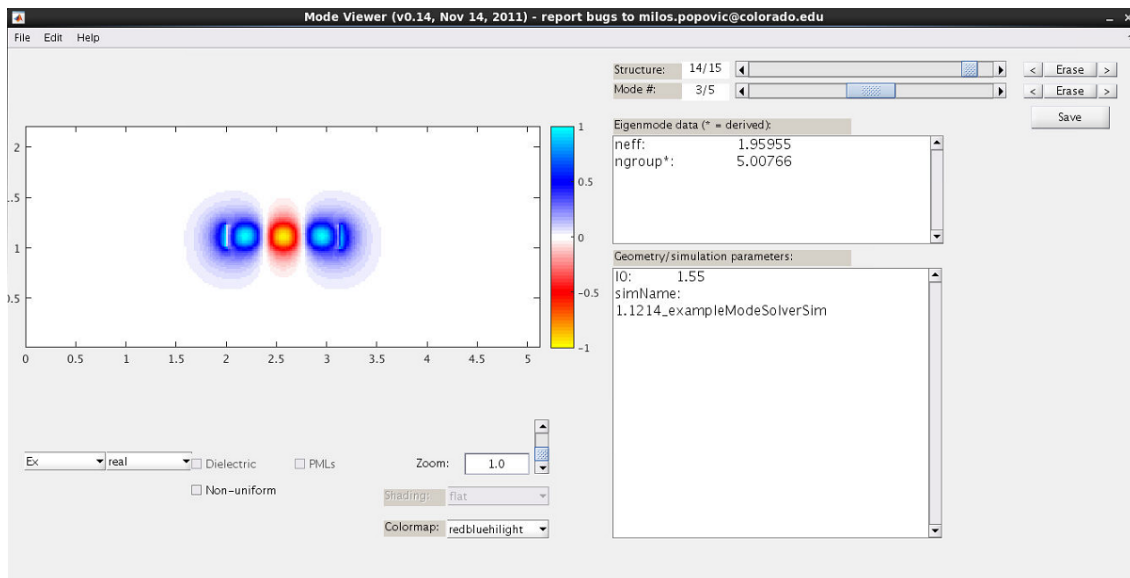


FIGURE 3.6: In this figure we can see the visualization tool for the mode solver. We can select the mode and the field components we want to visualize.

The first thing we can do is to visualize how the modes look like in a 2D cross section. First we are going to show the silicon oxide structure. We will see the first three modes: TE1, TE2, TM1. We are only plotting the real part of E_x and E_y . Those components gives us mostly of the information of the mode. TE1 has almost all the field on E_x by definition. However there is some E_y field on the edges due to edges effects. TE1 is

symmetrical respect to x and y axis in component E_x and asymmetrical respect to x and y in component E_y . We can see that the TE1 mode is well confined meaning that most of the field is inside the waveguide. TM1 is the only TM mode that can be guided using a 220nm thick waveguide. We can see that is not well confined and has even symmetry in component E_y and odd symmetry in component E_x . Finally for this width we can observe how TE2 appears. This mode is starting to be guided but if we want to guide it properly we will need a wider waveguide. We know that a mode is guided if we can see its shape clearly on the electric field plot. An other way to see if the mode is guided is look at the dispersion plot FIGURE 3.9 and 3.10 This mode has one null, even parity respect to x and odd parity respect to y in component E_x .

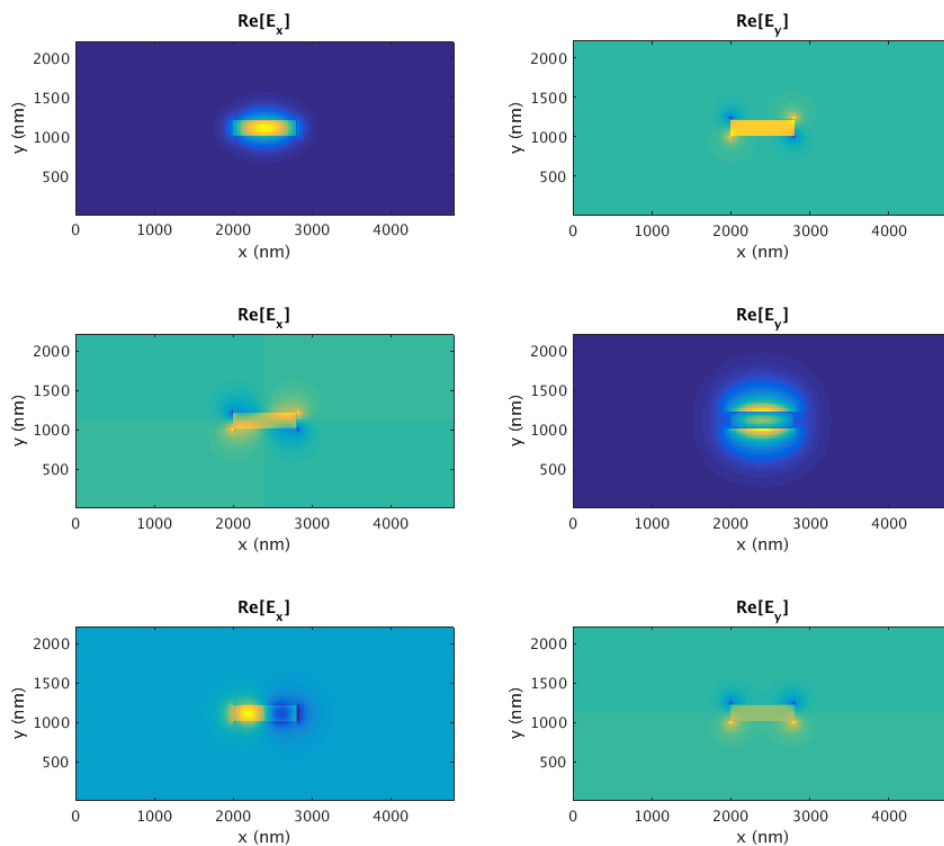


FIGURE 3.7: First three modes, first row TE1 second row TM1 third row TE2. 220 nm thick silicon waveguide on silicon oxide substrate and silicon oxide cladding.

Putting air as a cladding breaks the symmetry. This makes to loss the symmetry in the modes too. The index contrast is higher and the modes are better confined. The propagation constants are higher respect to silicon cladding.

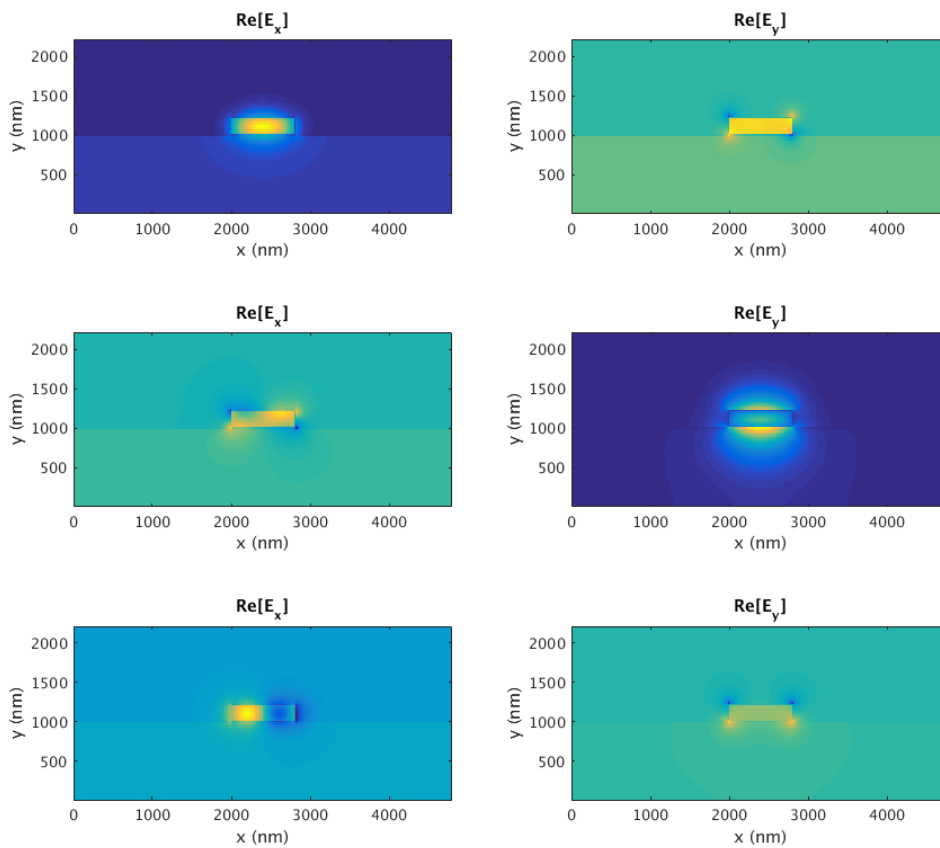


FIGURE 3.8: First three modes, first row TE1 second row TM1 third row TE2. 220 nm thick silicon waveguide on silicon oxide substrate and air cladding.

We have seen that the monomode cutoff for a two dimensional silicon waveguide surrounded by air is 200nm. Analogously we can compute the dispersion for air cladding and silicon oxide cladding. It is crucial for our designs to find the monomode cutoff. To avoid problems we are going to use monomode waveguides. After the simulations this results have been found:

Monomode cutoff width	
<i>SiO₂</i> cladding	400nm
<i>Air</i> cladding	600nm

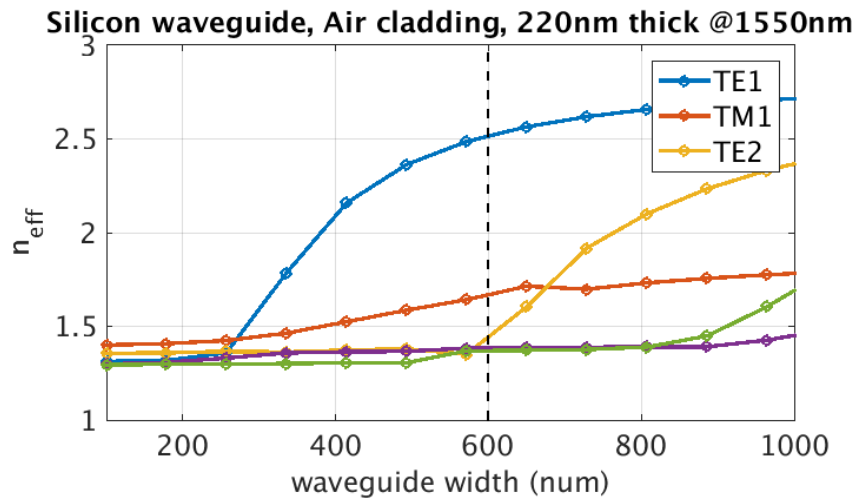


FIGURE 3.9: Dispersion of 220 nm thick silicon waveguide on silicon oxide substrate and air cladding.

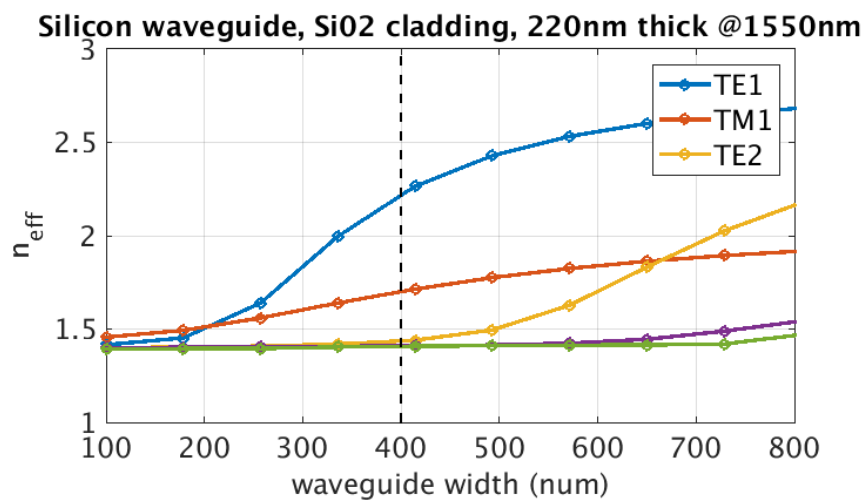


FIGURE 3.10: Dispersion of 220 nm thick silicon waveguide on silicon oxide substrate and silicon oxide cladding.

3.3 Coupled mode theory

In the last section we understood the single waveguide. Now we are going to see what happens when we put two waveguides close together. In order to understand that first we need to derive a mathematical theory called coupled mode theory. This theory is an approximation but it leads to pretty accurate results.

Every wave propagating through the structure can be written as a linear combination of all the modes in the structure. Because, as we have said before, the modes are a complete set. Without losing generality for now on we are going to focus only on TE modes. Since we are using monomode waveguides we are going to consider the fundamental TE mode.

We start with two wave guides, they can be different. Just for fun we will pick a rectangular waveguide and a heart shaped waveguide. As we can see in the following figure each wave guide will have its own fundamental mode.

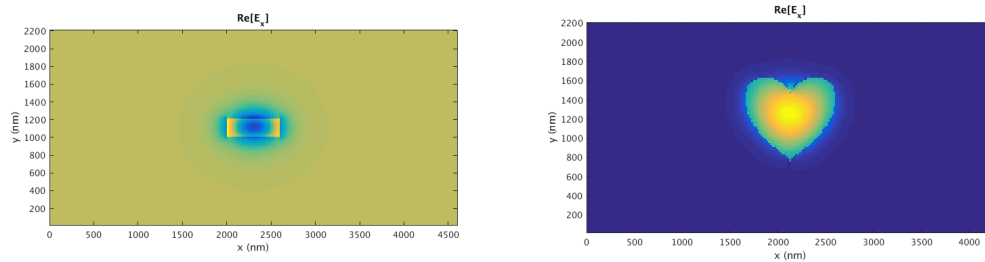


FIGURE 3.11: TE fundamental mode in both waveguides.

We can write the mode solution as a mode profile with a constant transversal shape propagating along the waveguide as:

$$\begin{aligned}
 \mathbf{E}_{\heartsuit} &= \mathbf{E}_{0,\heartsuit}(x, y)e^{-j\beta_{\heartsuit}z} \\
 \mathbf{H}_{\heartsuit} &= \mathbf{H}_{0,\heartsuit}(x, y)e^{-j\beta_{\heartsuit}z} \\
 \mathbf{E}_{\square} &= \mathbf{E}_{0,\square}(x, y)e^{-j\beta_{\square}z} \\
 \mathbf{H}_{\square} &= \mathbf{H}_{0,\square}(x, y)e^{-j\beta_{\square}z}
 \end{aligned} \tag{3.16}$$

Now we are going to couple these modes. When two waveguides are in close proximity, they become coupled. In the following figure we can see how the modes look like when the two waveguides are close. We can observe that the modes have slightly changed in shape.

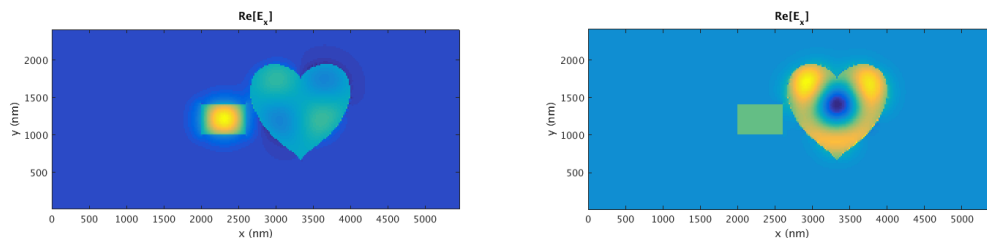


FIGURE 3.12: First two modes in the supermode picture.

This is called supermode picture. This two modes from the entire structure are the supermodes. This modes are going to be key in the following sections.

The assumption to derive the coupled mode theory is that the supermodes can be represented as a weighted sum of the individual guided modes. This implies that the modes do not change at all with the introduction of the second guide. In reality, the modes are deformed slightly, but are still coupled.

$$\begin{aligned}\mathbf{E} &= A(z)\mathbf{E}_\heartsuit + B(z)\mathbf{E}_\square \\ \mathbf{H} &= A(z)\mathbf{H}_\heartsuit + B(z)\mathbf{H}_\square\end{aligned}\quad (3.17)$$

Now we substitute these fields into Maxwell's curl equations (3.3) to obtain

$$(\hat{z} \times \mathbf{E}_\heartsuit) \frac{dA}{dz} + (\hat{z} \times \mathbf{E}_\square) \frac{dB}{dz} = 0 \quad (3.18)$$

$$(\hat{z} \times \mathbf{H}_\heartsuit) \frac{dA}{dz} - j\omega\epsilon_o(\epsilon_r - \epsilon_\heartsuit)A\mathbf{E}_\heartsuit + (\hat{z} \times \mathbf{H}_\square) \frac{dB}{dz} - j\omega\epsilon_o(\epsilon_r - \epsilon_\square)A\mathbf{E}_\square = 0 \quad (3.19)$$

We derive the generalized coupled-mode equations by substituting the above expressions into the following integral equations.

$$\begin{aligned}\int_{-\infty}^{\infty} \int_{-\infty}^{\infty} [\mathbf{E}_\heartsuit^* \bullet (Eq.4.18) - \mathbf{H}_\square^* \bullet (Eq.4.19)] dx dy &= 0 \\ \int_{-\infty}^{\infty} \int_{-\infty}^{\infty} [\mathbf{E}_\square^* \bullet (Eq.4.18) - \mathbf{H}_\heartsuit^* \bullet (Eq.4.18)] dx dy &= 0\end{aligned}\quad (3.20)$$

After lots of algebra, we get the generalized coupled-mode equations. These are solved to describe the coupling between the two waveguides.

$$\begin{aligned}\frac{dA}{dz} + c_{\heartsuit\square} \frac{dB}{dz} e^{-j(\beta_\square - \beta_\heartsuit)z} + j\chi_\heartsuit A + j\kappa_{\heartsuit\square} B e^{-j(\beta_\square - \beta_\heartsuit)z} &= 0 \\ \frac{dB}{dz} + c_{\square\heartsuit} \frac{dA}{dz} e^{-j(\beta_\square - \beta_\heartsuit)z} + j\chi_\square B + j\kappa_{\square\heartsuit} A e^{-j(\beta_\square - \beta_\heartsuit)z} &= 0\end{aligned}\quad (3.21)$$

Where $\kappa_{\heartsuit\square}$ is the mode coupling coefficient

$$\kappa_{\heartsuit\square} = \frac{\omega\epsilon_o \int_{-\infty}^{\infty} \int_{-\infty}^{\infty} (\epsilon_r - \epsilon_\square) \mathbf{E}_\heartsuit^* \bullet \mathbf{E}_\square dx dy}{\int_{-\infty}^{\infty} \int_{-\infty}^{\infty} \hat{z} \bullet (\mathbf{E}_\heartsuit^* \times \mathbf{H}_\square + \mathbf{E}_\square \times \mathbf{H}_\heartsuit^*) dx dy} \quad (3.22)$$

$c_{\heartsuit\square}$ is the butt coupling coefficient

$$c_{\heartsuit\square} = \frac{\int_{-\infty}^{\infty} \int_{-\infty}^{\infty} \hat{z} \bullet (\mathbf{E}_\heartsuit^* \times \mathbf{H}_\square + \mathbf{E}_\square \times \mathbf{H}_\heartsuit^*) dx dy}{\int_{-\infty}^{\infty} \int_{-\infty}^{\infty} \hat{z} \bullet (\mathbf{E}_\heartsuit^* \times \mathbf{H}_\heartsuit + \mathbf{E}_\heartsuit \times \mathbf{H}_\heartsuit^*) dx dy} \quad (3.23)$$

χ_\heartsuit is the change in propagation constant

$$\chi_\heartsuit = \frac{\omega\epsilon_o \int_{-\infty}^{\infty} \int_{-\infty}^{\infty} (\epsilon_r - \epsilon_\heartsuit) \mathbf{E}_\heartsuit^* \bullet \mathbf{E}_\heartsuit dx dy}{\int_{-\infty}^{\infty} \int_{-\infty}^{\infty} \hat{z} \bullet (\mathbf{E}_\heartsuit^* \times \mathbf{H}_\heartsuit + \mathbf{E}_\heartsuit \times \mathbf{H}_\heartsuit^*) dx dy} \quad (3.24)$$

χ_\square will be the same expression (3.24) but changing hearts to squares.

Where ϵ_r is the dielectric function containing both waveguides and ϵ_\square is the dielectric with only \square waveguide.

The most important coefficient is the coupling coefficient. This parameter quantifies how efficiently power leaks from waveguide \heartsuit to waveguide \square due to the behavior of the supermode. If we change \heartsuit for \square and \square for \heartsuit . We will get a coupling coefficient that tells how efficiently power leaks from \square to \heartsuit .

The coefficient $c_{\heartsuit\square}$ quantifies the excitation efficiency from one waveguide to an other. If the waveguides are sufficient separated then $c_{\heartsuit\square} \approx 0$ and $\kappa_{\heartsuit\square} \approx 0$.

Finally the coefficient χ_\heartsuit measure how change the propagation velocity of \heartsuit due to the fact that \square is close. This coefficient increases as the gap between waveguides is smaller. Normally we will neglect this term because is much lower than the other two.

We know that the total power in wave guide \heartsuit is

$$P_\heartsuit = \frac{1}{2} \int_{-\infty}^{\infty} \int_{-\infty}^{\infty} [\mathbf{E}_\heartsuit \times \mathbf{H}_\heartsuit^*] \cdot \hat{z} dx dy \quad (3.25)$$

The observe that the denominator in all the coefficients is equal to $4P_\heartsuit$. Without losing generality we will normalize the power according to $4P_\heartsuit = 1$. Then can be shown that $c_{\heartsuit\square} = c_{\square\heartsuit}^*$ and $\chi_\heartsuit = \chi_\square^*$.

If we substitute the fields on equation (4.25) and we work with the algebra we will find the following expression for the power:

$$P = \frac{1}{4} [|A|^2 + |B|^2 + A^* B c_{\heartsuit\square} e^{-j2\delta z} + AB^* c_{\square\heartsuit}^* e^{j2\delta z}] \quad (3.26)$$

where $\delta = \frac{\beta_\square - \beta_\heartsuit}{2}$. Assuming that the waveguides are loss-less the power has to be conserved and so

$$\frac{dP}{dz} = 0 \quad (3.27)$$

$$jA^* B (\kappa_{\heartsuit\square}^* - \kappa_{\square\heartsuit} - 2\delta c_{\heartsuit\square}) e^{-j2\delta z} - jAB^* (\kappa_{\square\heartsuit} - \kappa_{\heartsuit\square}^* - 2\delta c_{\square\heartsuit}^*) e^{-j2\delta z} = 0 \quad (3.28)$$

And this has to be satisfied for all z, then we must have $\kappa_{\square\heartsuit} = \kappa_{\heartsuit\square}^* + 2\delta c_{\heartsuit\square}^*$. Then if the waveguides are similar and not super close then $\kappa_{\square\heartsuit} = \kappa_{\heartsuit\square}^*$. In our heart shape waveguide example we could not be able to neglect $c_{\heartsuit\square}$ but since we are going to use square similar waveguides we can assume $c_{\heartsuit\square} = \chi_\heartsuit = 0$. Finally after a lot of effort we found the coupled-mode equations.

$$\begin{aligned} \frac{dA}{dz} &= -j\kappa_{\heartsuit\square} B e^{-j(\beta_\square - \beta_\heartsuit)z} \\ \frac{dB}{dz} &= -j\kappa_{\square\heartsuit} A e^{-j(\beta_\square - \beta_\heartsuit)z} \end{aligned} \quad (3.29)$$

This simple equations describe how the power bounces around from one mode to an other [15].

3.4 Directional Coupler

In the last section we have derived the basic equations for the coupling mode theory. We also introduced key concepts such as the coupling coefficient. Now we have the tools to study the directional coupler. First we are going to approach the directional coupler analytically using coupled mode theory and finally we are going to use finite differences in time domain to solve numerically the problem.

3.4.1 Directional Coupler: CMT approach

In a directional coupler we have two parallel waveguides. Those waveguides are separated by a gap g . They have width w_1, w_2 . And they can be air or silicon oxide cladding with a thick t .

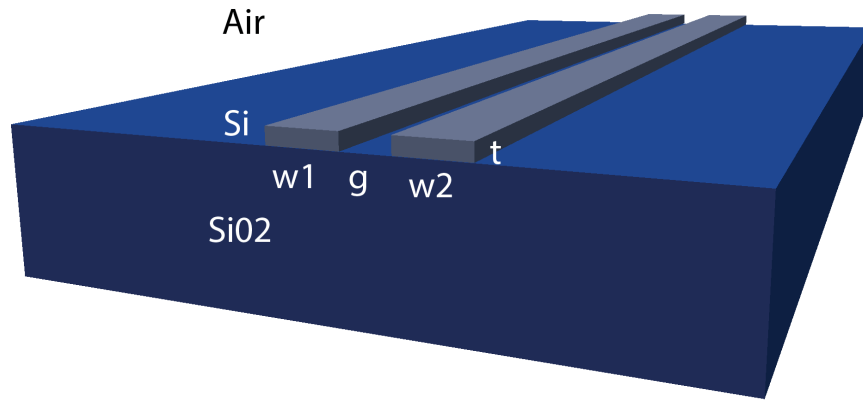


FIGURE 3.13: Directional coupler

We start injecting light in one of the wave guides. Then the initial conditions to solve equation (4.29) will be $A(0) = A_0$ and $B(0) = 0$. Therefore is trivial to get the solutions for the directional coupler.

$$\begin{aligned} A(z) &= A_o \left[\cos(\psi z) + \frac{j\delta}{\psi} \sin(\psi z) \right] e^{-j\delta z} \\ B(z) &= -A_o \frac{j\kappa}{\psi} \sin(\psi z) e^{j\delta z} \end{aligned} \quad (3.30)$$

where $\kappa = \kappa_{AB} = \kappa_{BA}^*$, $\delta = \beta_B - \beta_A$ and $\psi = \sqrt{\kappa^2 + \delta^2}$.

It makes more sense to express the last expression in terms of power

$$\begin{aligned} P_A(z) &= \frac{|A(z)|^2}{|A_o|^2} = 1 - F \sin^2(\psi z) \\ P_B(z) &= \frac{|B(z)|^2}{|B_o|^2} = F \sin^2(\psi z) \end{aligned} \quad (3.31)$$

Where F is the maximum power-coupling efficiency

$$F = \left(\frac{\kappa}{\psi}\right)^2 = \frac{1}{1 + \left(\frac{\delta}{\kappa}\right)^2} \quad (3.32)$$

From the expression for power-coupling efficiency we can deduce that we will only be able to transfer all the power from one waveguide to the other if $\frac{\delta}{\kappa} = 0$. This can happen if $\kappa \gg \delta$, i.e. waveguides with similar sizes and close together. However if the waveguides get closer and closer then the approximations we have done are less valid. The other way to be able to achieve 100% power transfer is using the same exact width for both waveguides.

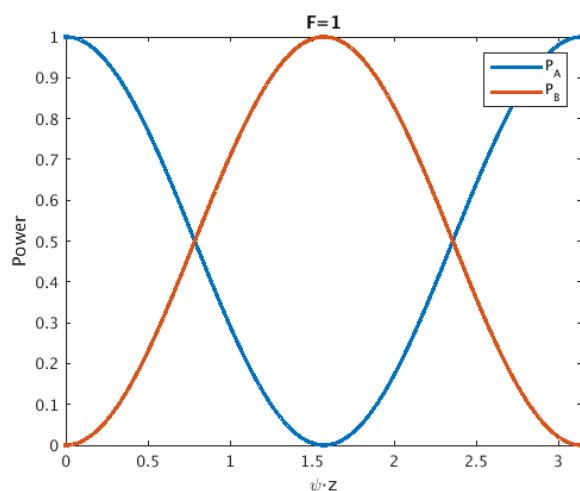


FIGURE 3.14: Power in each mode vs z with $F=1$

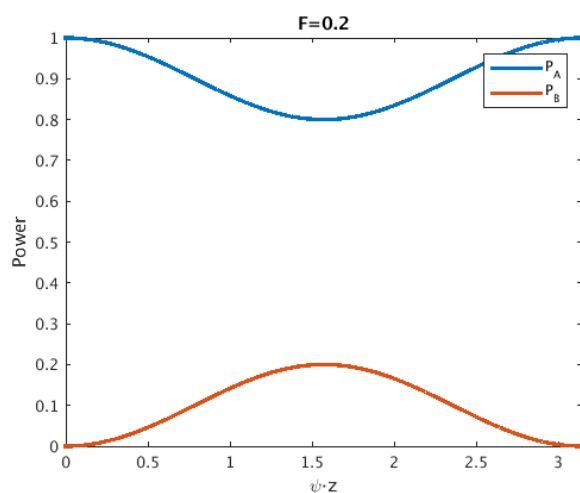


FIGURE 3.15: Power in each mode vs z with $F=0.2$

The aim of this section is design a directional coupler. A directional coupler is a device in which we excite one of the two inputs and we get half of the power in both outputs. In order to do that we will chose for which z we have 50-50 power transfer and then

we will pick this value as the length of the device.

$$L_{3dB} = \frac{1}{\psi} \operatorname{asin}\left(\frac{1}{\sqrt{2F}}\right) = \frac{\operatorname{asin}\left(\sqrt{\frac{1+(\frac{\delta}{\kappa})^2}{2}}\right)}{\sqrt{\kappa^2 + \delta^2}} \quad (3.33)$$

This equation has solution if $F > 0.5$ otherwise we can not achieve 50% transmission from the first waveguide to the second. This condition leads to a condition for δ and κ .

$$\delta \leq |\kappa| \quad (3.34)$$

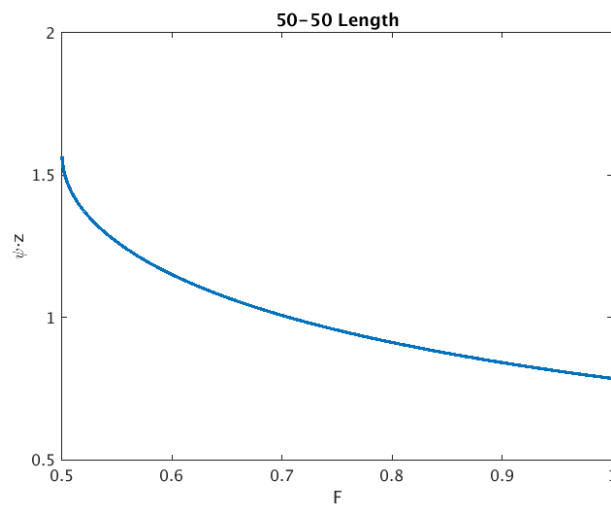


FIGURE 3.16: [Plotting equation 4.33 $L_{3dB}\psi-F$]

If $F = 1$ we have a directional coupler. For $F < 1$ we have a delta-beta coupler. For the case $F = 0.5$ we do not need exactly L_{3dB} to make the device work 50-50 because it is first order invariant with length. That would be like FIGURE 3.15 and we would chose the length that gives a maximum. So we just need to be close enough to that length.

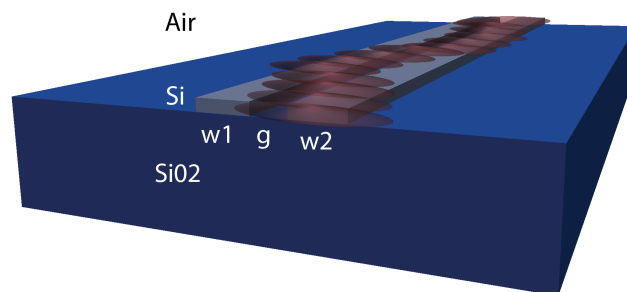


FIGURE 3.17: Artistic representation of our beamsplitter. We start with all the power in one wavguide then it starts bouncing form one waveguide to the other. Every period we can find a length which splits perfectly the power.

3.4.2 Directional Coupler: FDTD approach

We have seen the theory behind the directional coupler. The fact is, if we want to design a real device we should verify our geometry first with a more accurate way than CMT. One of the best ways to simulate the propagation of electromagnetic waves through dielectrics is finite differences time domain, or FDTD. This approach breaks down the domain in cells and compute the interaction between neighbors. It is a really elegant way to simulate this kind of systems. There are some commercial software that are able to do FDTD simulations. However we have been using the code wrote partially by Prof. Miloš Popović and company.

The code is written in fortran. However, a few years ago, a matlab script that runs the simulation had been created. So now is much simpler to do the simulations. For every simulation we have to define the structure in a three dimensional matrix, the positions of the sources and the position for the observation plains. The code can work in 2D supposing one dimension infinite (i.e. slab waveguides) or 3D. We did the study considering 2D just because the simulations took less time. We will skip the 3D results and we will see directly the results in 2D. They are analogous to 3D.

The aim is simulating low-loss couplers. To do that we want to avoid something called numerical scattering. The numerical scattering is caused due to the discretization. If the discretization is small enough we will not have numerical scattering. However, the minimum discretization that we can use to solve the structure in a reasonable time and not consume all the resources of the server is $dx = 10nm$. In order to solve that problem we will use a Fermi-Dirac distribution to smooth the edges.

There is no specific reason to use a Fermi-Dirac distribution instead of other function besides it works. When I arrived at the lab they were already using this technique to reduce the numerical scattering.

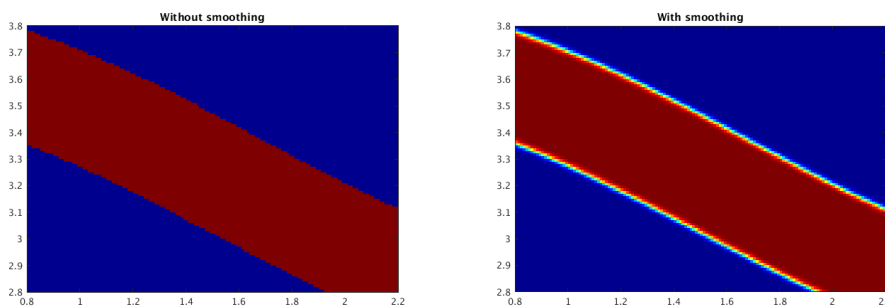


FIGURE 3.18: On the left: waveguide without smoothing. On the right: smoothed waveguide

The Fermi-Dirac equation that we are using to smooth the edges is

$$y = \frac{1}{1 + \ln(9)e^{\frac{ax}{1.5dy}}} \quad (3.35)$$

where a is a parameter that controls how many pixels are going to be smoothed. The smoothing should be performed perpendicular to the curve at each point. However,

we apply the smoothing in y direction since is the mostly affected direction due to discretization.

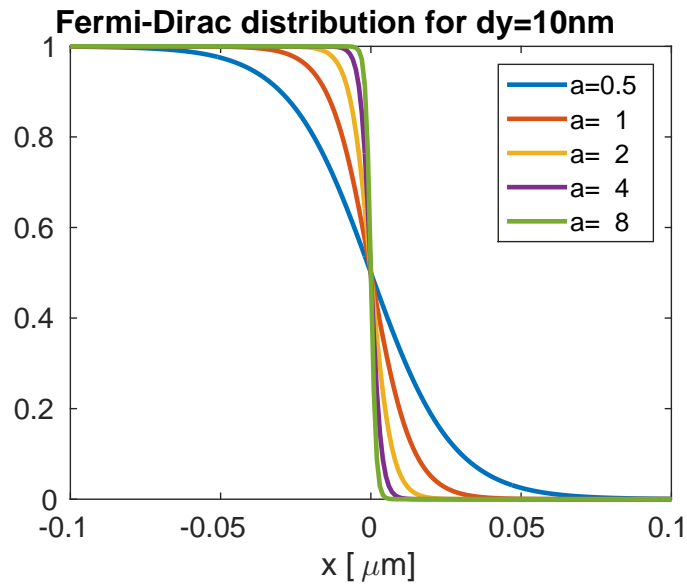


FIGURE 3.19: Fermi-Dirac distribution for different values of a .

We want to see the effect of the smooth parameter on the dielectric. We have simulated a sinusoidal bend using the FDTD code. We keep track of the losses on the structure while changing the parameter a . For now on we are going to chose a value of $a = 1$ since give us low loss.

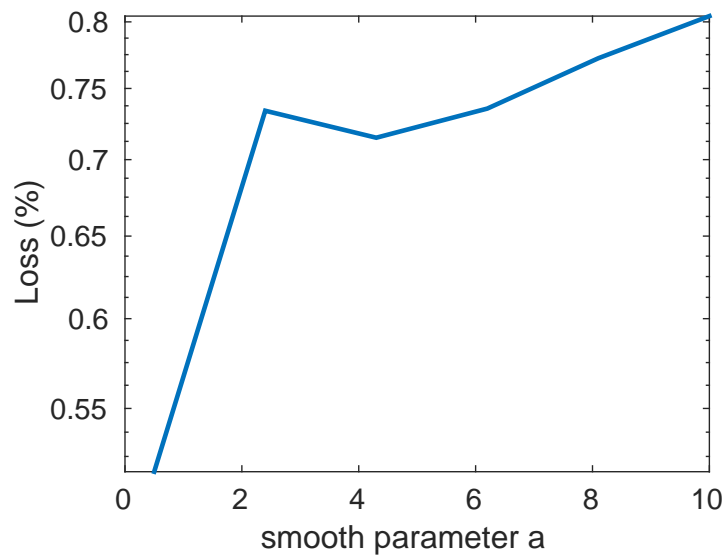


FIGURE 3.20: Loss in the structure versus the smooth parameter a .

In order to simulate the directional coupler we will add a bending input and bending output. This sinusoidal bends will couple some light when we get closer to the coupling region. Therefore we have to modify the coupling equation in order to take into account this extra coupling due to the bend region. Then we will have the cross port power K^2 and the through port power T^2 .

$$\begin{aligned} K^2 &= \sin\left(\frac{\pi}{2L_z}[L + z_{bend}]\right)^2 \\ T^2 &= \cos\left(\frac{\pi}{2L_z}[L + z_{bend}]\right)^2 \end{aligned} \quad (3.36)$$

Where L_z is the cross-over length and z_{bend} represents the effective extra coupler distance introduced by the coupling from the non-parallel waveguides.

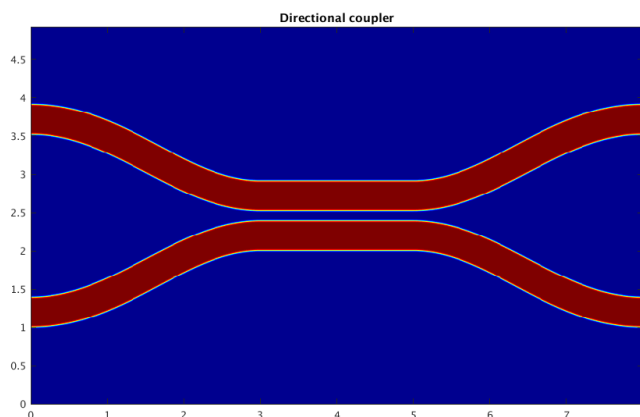


FIGURE 3.21: Directional coupler dielectric.

Now we can simulate the directional coupler for different lengths and fit the curve to the theoretical equation. In this way we can find L_z, z_{bend} . We will chose air cladding and 160nm width for both waveguides.

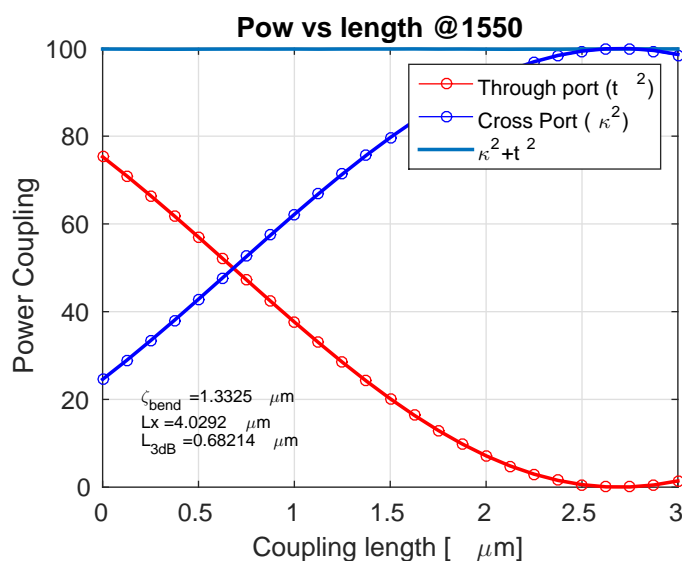


FIGURE 3.22: Directional coupler: power versus length.

Once we found the desired length to make the device work as a beamsplitter we can look at its dependence with wavelength. As we can see in the figure the transmission coefficients highly depend on wavelength. So, the directional coupler can be a short beamsplitter but not a broadband.

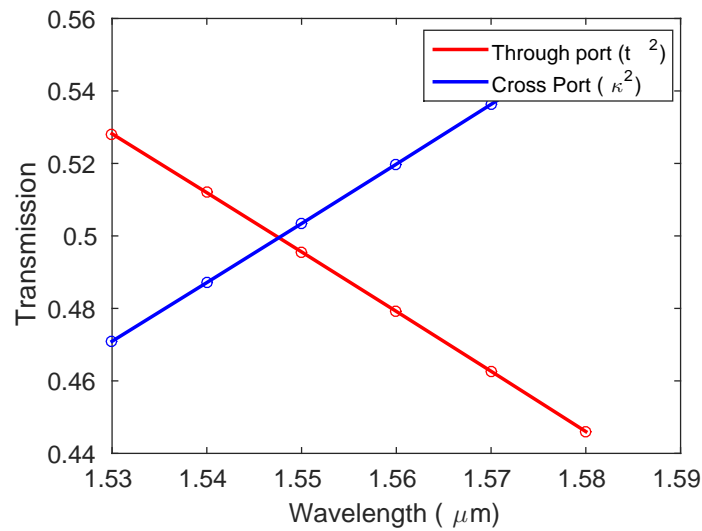


FIGURE 3.23: Directional coupler: power versus wavelength at 50-50 length.

A variation of the directional coupler is the delta-beta directional coupler. As we have seen before if we make the waveguides width different then we can not achieve 100% power transfer from one waveguide to the other one. Just to remember the cross port power transfer.

$$K^2 = \frac{\sin^2(\kappa L \sqrt{1 + (\frac{\Delta\beta}{2\kappa})^2})}{1 + (\frac{\Delta\beta}{2\kappa})^2} \quad (3.37)$$

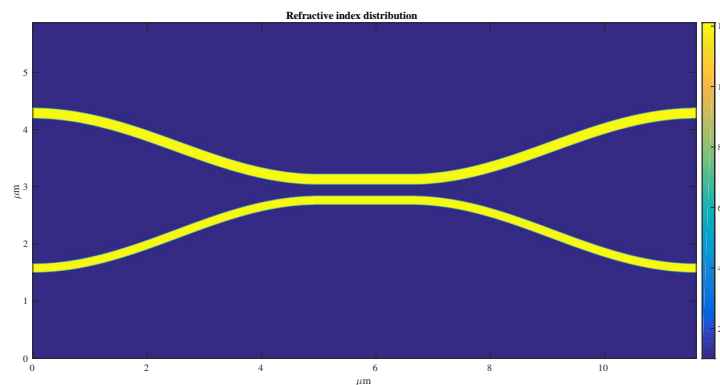


FIGURE 3.24: Delta-Beta Directional coupler dielectric.

Using this principle we can find the width that make exactly 50% power transfer at maximum. As we saw in the last section. In this way we can design a structure first order invariant respect to length. We chose air cladding and 180 and 150 nm width.

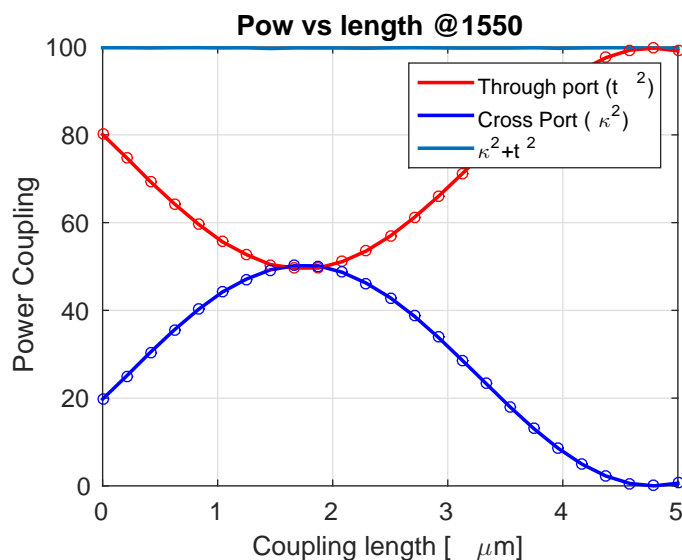


FIGURE 3.25: Delta-Beta Directional coupler: power versus length.

So we chose length $1.6\mu m$ and we can see that as the directional coupler is highly dependent on wavelength.

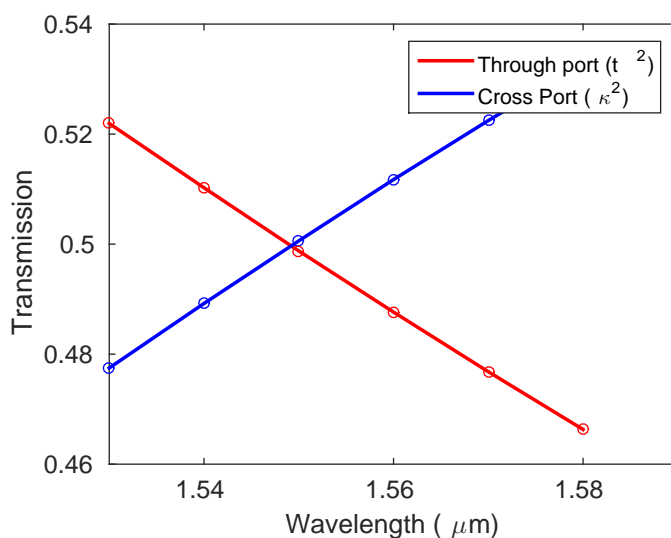


FIGURE 3.26: Delta-Beta Directional coupler: power versus wavelength at 50-50 length.

3.4.3 Mach-Zehnder interferometer

As we have seen on 2.2 MZI are key devices to manipulate qubits. We have already shown they transfer matrix 2.25. In this section we will show measurements performed

on a integrated MZI. Those chips have been created by Jeff Shainline. To build those devices we need to do a template first (FIGURE 3.27). The shape is coded in python and the output is a .gds file that has the geometry to builder the device. Then the device is built by lithography in a clean room.

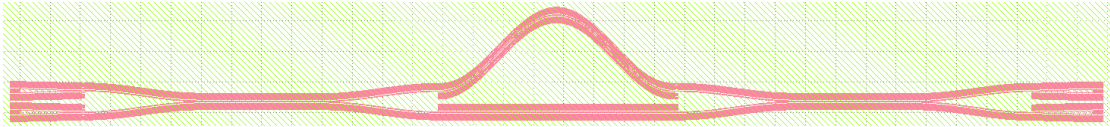


FIGURE 3.27: MZI template made by Jeff Shainline.

In contrast to the devices I described, the core of this device is made by SiN₂ and the cladding is air. Just to remember a MZI is formed of three pieces, first a 50-50 directional coupler, secondly a phase shift between paths and thirdly an other 50-50 directional coupler. The phase shift can be active or passive. When the phase shift is active a resistor is used to heat up one of the paths to change the refractive index and so the propagation constant. In contrast for passive phase shifts we just change the length between both paths. In a In FIGURE 3.28 we can see two pipes on the very right and very left of the image. Those pipes are the optical fibers providing and receiving the laser light. We can also see two ports at each side. In this case we will measure left top right bottom. We can also see in the middle two different path length for the top and bottom waveguide.

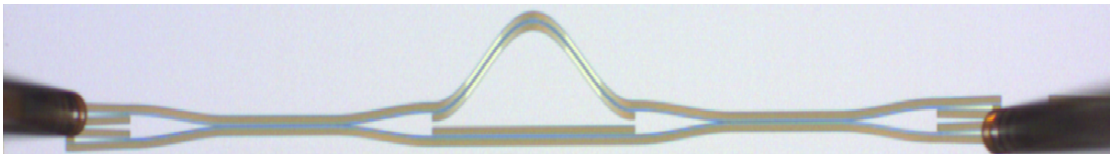


FIGURE 3.28: The image is showing a augmented view of a MZI on SiN₂ it is taken by myself.

If we zoom in close to the fiber we will see a tape structure called grading. A grading is used to couple the light from the fiber to the chip. We can also see that apart of the thin waveguides we have a thick walls next to them. Those walls are not needed but help on lithography process (FIGURE 3.29).

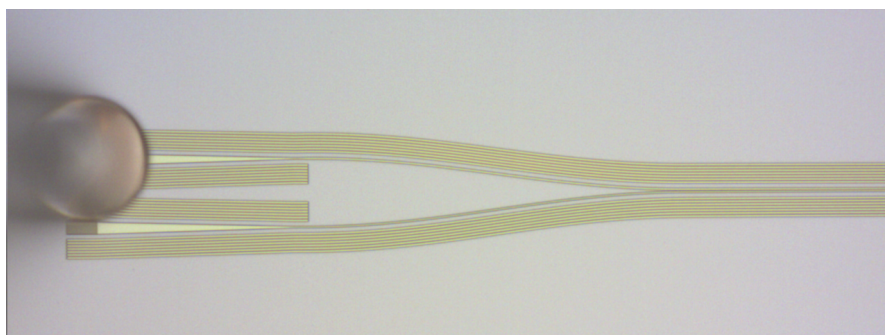


FIGURE 3.29: The image is showing a detailed augmented view of the left part of a MZI on NSiO₂ it is taken by myself.

Now we shine 1mW of light through one fiber and we read the output using a photodetector. We have a polarization controller or PC to change the fiber polarization and reduce the losses. We can also move the fibers around the chip using a very precise micrometer. We want to put the fiber in the position and set the polarization that maximizes the power transfer through the device. Once we do that we can start measuring. The laser will shift the wavelength and measure the power transfer at each wavelength. Then we change the ports and repeat the process.

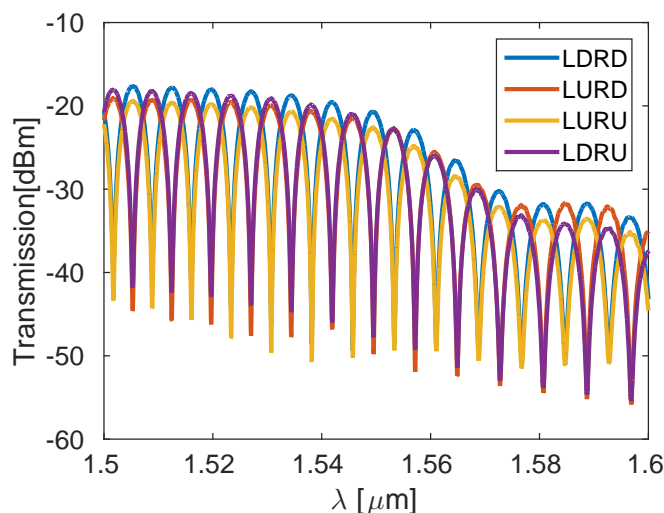


FIGURE 3.30: Transmission for all ports combinations. The signals are coded as the following: left (L) followed by up or down (U or D) and then R followed by up or down (U or D). For example the code LDRU means input port: left down, output port: right up.

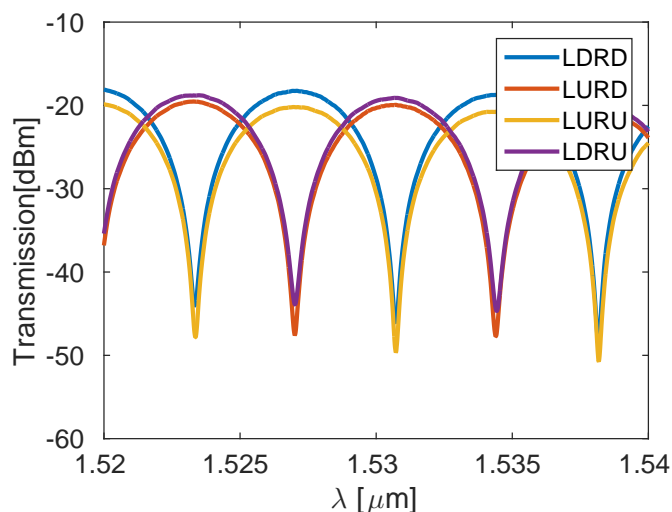


FIGURE 3.31: Transmission for all ports combinations. The signals are coded as the following: left (L) followed by up or down (U or D) and then R followed by up or down (U or D). For example the code LDRU means input port: left down, output port: right up.

The result should be a sinusoidal of transmission versus wavelength. Changing the wavelength with a fix length is the same as fixing the wavelength and changing the length. But the first is easier to do. The second one we should measure different devices with different lengths. We can see that for large wavelengths the device stops working this is due to the fact that the grading stop working at those wavelengths. We can also see that the difference from the minimum to the maximum is 30dB. We need about 37dB extinction to guarantee 49/51 couplers (FIGURE 3.30).

We should expect the same transmission for cross ports, in reality is hard to achieve it just because optimize the fiber position in different places but in the same way is really difficult (FIGURE 3.31).

3.5 Adiabatic coupler

So far we have talked about fixed structures. In those structures the waveguide width does not change with the propagation direction. In this section we are going to explore what happen when we change the geometry in z direction. We will use those results to design an another kind of coupler, the adiabatic coupler.

We have already talk about the orthogonality condition in modes. This condition can not be satisfied in waveguide structures in which the waveguide parameters vary in the direction of propagation. It can not be satisfied in the sense that we can not find the same base of ortogonal modes at each distance if it is changing in z direction. However we can define the local normal modes at the position z_0 . The local normal mode representation will now become a function of z .

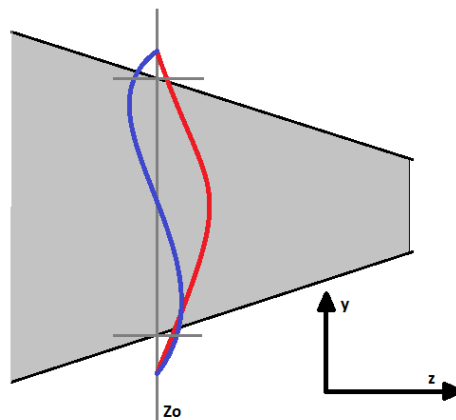


FIGURE 3.32: To define a local normal mode, the slowly varying waveguide structure (darker line) is replaced at z_0 by the structure constant with z (less darker line), and the normal mode solutions at Z_0 are obtained.

The amplitudes of the local normal modes in a varying waveguide structure can vary in contrast to the fixed structure. Power transfer between the local normal modes of

a varying structure occurs, and we will see that the magnitude of that power transfer depends on the rate of change of the geometry of the structure.

We have to modify the coupled mode theory due to the variation in z . We are not going to derive the equations but a rigorous derivation can be found on [17]. The main idea to find the equations is write the mode of each local section in terms of the modes of the section right before. In this way we can find how many power is transmitted from z to $z + dz$.

$$\begin{aligned}\frac{\partial A_i}{\partial z} &= -C_{ij} \frac{\partial \rho}{\partial z} A_j + j\beta_i A_i \\ \frac{\partial A_j}{\partial z} &= -C_{ij} \frac{\partial \rho}{\partial z} A_i + j\beta_j A_j\end{aligned}\quad (3.38)$$

where the subscripts i and j refer to the fundamental and next higher order systems modes. Here $(A_i, A_j), (\beta_i, \beta_j)$ and C_{ij} are the corresponding amplitudes, propagation constants, and normalized coupling coefficient between these modes. The derivative $\frac{\partial \rho}{\partial z}$ is the rate of change of a general parameter related to the specific geometry of the structure [17]. In our case we are changing width and gap at the same time so we should find a smart way to define ρ . However we will solve the structure numerically so we are not going to use this formula in this section.

We define a slow or adiabatic waveguide transition as a transition between two waveguide structures that takes place so slowly that negligible power transfer occurs between the normal modes, as they propagate from one structure to the other. That happen when the rate of change of the walls is small in z direction. Then $\frac{\partial \rho}{\partial z} \rightarrow 0$ and no interaction appears between different modes.

$$\begin{aligned}\frac{\partial A_i}{\partial z} &= j\beta_i A_i \\ \frac{\partial A_j}{\partial z} &= j\beta_j A_j\end{aligned}\quad (3.39)$$

This happen if $\delta \gg \kappa$. Then we can launch the first mode A of the structure at $z = 0$ and ideally the power in the second mode B at length L will be

$$\frac{|B(L)|^2}{|A(0)|^2} \rightarrow 0 \quad (3.40)$$

This means that all the power will remind in the first mode. Notice that at each section the modes are changing. By adiabatic assumption the geometry will change slowly. However for a long structure we can start in one geometry and end in a completely different one. This is the key concept to design a low loss broad-band coupler.

We will start with two waveguides separated in order to not have coupling at all. We want the width of this two waveguides to be different. In this way the two first supermodes will have different propagation constants. The first mode will correspond to the wider waveguide. We want to change this cross section with a large gap and two waveguides with different width to a cross section with a small gap and two equal

waveguides. The modes in this last section will be the symmetrical and the antisymmetrical. If our structure is large enough to be adiabatic then the first mode at the beginning will lead to the first mode at the end. And the same for the second mode.

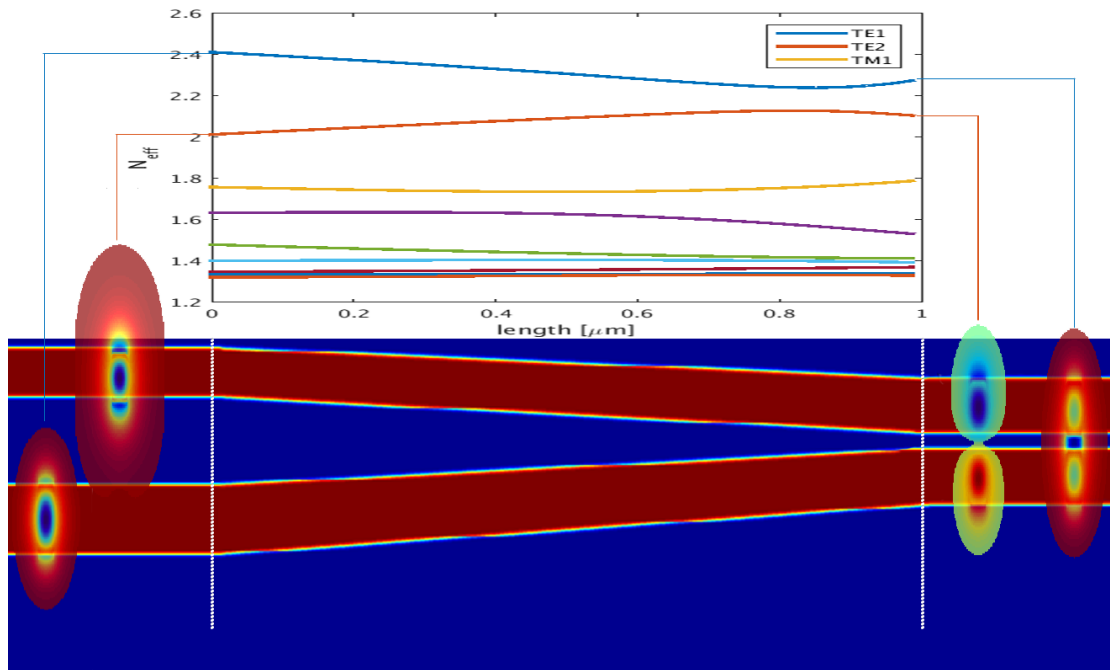


FIGURE 3.33: We can see how is the structure and which are the modes in the first and last section. We can also see how the propagation constant evolve with z .

If we have two equal waveguides and we have all the power in either the first mode or the second mode. Means that we have half of the power in each waveguide. Then we need to separate the two waveguides in a symmetrical way. By symmetry there is no way to transfer power from one waveguide to the other one if we have the symmetrical or antisymmetrical supermodes.

Despite these structures are robust, easy to design and have a really good performance they tend to be so long ($\sim 100\mu m$). This is not a problem if we do not care about space, but if we want to package a beamsplitters network we may have to use another kind of coupler.

We can not use FDTD to simulate those structures because they are too computationally intrusive. In order to simulate them we are going to use a film mode matching or FMM, written by Prof. Miloš Popović.

We are going to simulate only the adiabatic region. We are going to keep tracking of the power for each symmetrical and antisymmetrical mode. Ideally we want to pick the length that makes the power on the antisymmetrical mode zero. But for a real design we need the minimum length that makes the device work under some conditions. We

impose the minimum error ratio has to be 1% in power, so 49-51% is accepted. This means having less than $1e-4$ of the normalized power in the antisymmetrical mode.

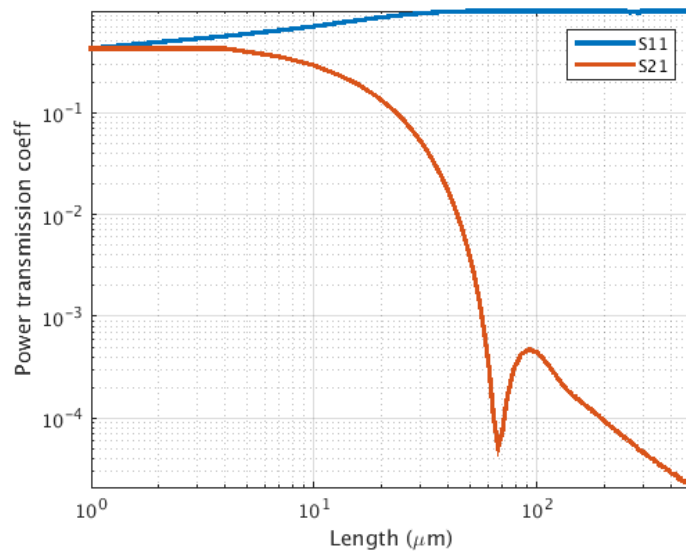


FIGURE 3.34: Observation plain: last section where the two waveguides are the same width. We can see the rate of power for the symmetrical mode and the antisymmetrical.

From the plot we can see that at length near to $70\mu m$ the device could work. However this length is really sensitive, a little change on length is going to change a lot the fraction of power in the antisymmetrical mode. In order to avoid that we would pick a length higher than $20\mu m$ which is really long.

3.6 Zero Xtalk coupler

Until now we have seen two of the three main coupler strategies. We are missing the multimode interference, or MMI but we are not going to cover this last one in this thesis. The directional coupler is really short $\sim 5\mu m$ but is highly wavelength dependent. In opposition to the adiabatic coupler which is really long $\sim 200\mu m$ but is really broadband. So what we are going to do in this section is design a coupler which is short and broadband. In order to do that we are going to use concepts from both directional and adiabatic coupler and we are going to create and hybrid. The key idea to this design came from my advisor Prof. Miloš Popović when he was doing his Ph.D. at MIT back in 2005. One day he was trying his FMM code, he was simulating the same kind of adiabatic coupler we saw in the last section but he was trying to tilt that structure. Surprisingly he found that the coupling from one section to the next one changes with tilting. But even more, changing the tilting direction changes the sign of the coupling coefficient. Which means that exist a tilt of the structure that makes the coupling from the first to the second mode zero. So now instead of trying to change slowly the structure to avoid coupling what we want to do is tilt it to compensate the coupling for one mode to the other.

The design will consist in the following geometry. We start with a fat waveguide and a thin waveguide. In this way we can separate the propagation constant from the first and second mode. Then keeping the gap constant we go from different width to the same width. We do this transition linearly. In the last cross section if we have the first or second mode the light will be split equally between waveguides.

First we have to chose the parameters for $w1(0), w1(L), w2(0), w2(L)$ and g . The number of degrees of freedom is 3 for the first section and 2 for the last section. We are going to simulate the first and last section and see how the geometry change the effective index of the three first modes. In order to help this process we not only want to avoid coupling from the first to the second mode but also from the second to the third. The condition then is to find the geometry that give us the maximum distance from N_{eff1}, N_{eff2} and N_{eff2}, N_{eff3} . This means that $N_{eff2} - N_{eff1} \approx N_{eff3} - N_{eff2}$.

We are going to use silicon cladding structures for the 3D simulations. The reason for that is to simplify the problem. Having a horizontal symmetry on the cross section avoid coupling from TE to TM modes. Then we only have to worry bout TE modes. The number of degrees of freedom is 3 for the first section and 2 for the last section. So, we will start with the last section since it is easier. After simulating the cross section we realized that roughly as small the gap the better. Then we pick a $g = 100nm$ since is the smallest gap we can fabricate without any problems. Then we consider which width pick. We know that $w1(L) = w2(L)$ to have the symmetrical mode in the last section. After plotting the effective index for the three first modes we decided that the best with is $w(L) = 380nm$. Then by trial and error we find that the best width are $w1(0) = 480nm$ $w2(0) = 340nm$.

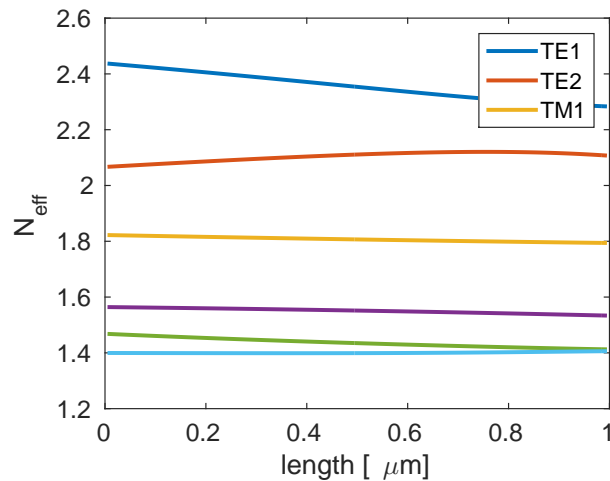


FIGURE 3.35: N_{eff} versus length for the following geometry: $w1(0) = 480nm$, $w2(0) = 340nm$, $w(L) = 380nm$, $g = 100nm$. Notice that the N_{eff} does not depend on the tilting.

We start the algorithm to design the structure with only the first cross section. We

compute the modes on this section with the FMM code. Then we introduce a new layer. The widths on this layer will be slightly different since we moved a step in z direction. Then we are going to slide this layer in x direction an amount ρ . If we plot the coupling from the first mode in the first section to the second mode in the second section and the second mode in the first section and the first mode in the second section we see that there is a ρ_0 which makes this amount zero.

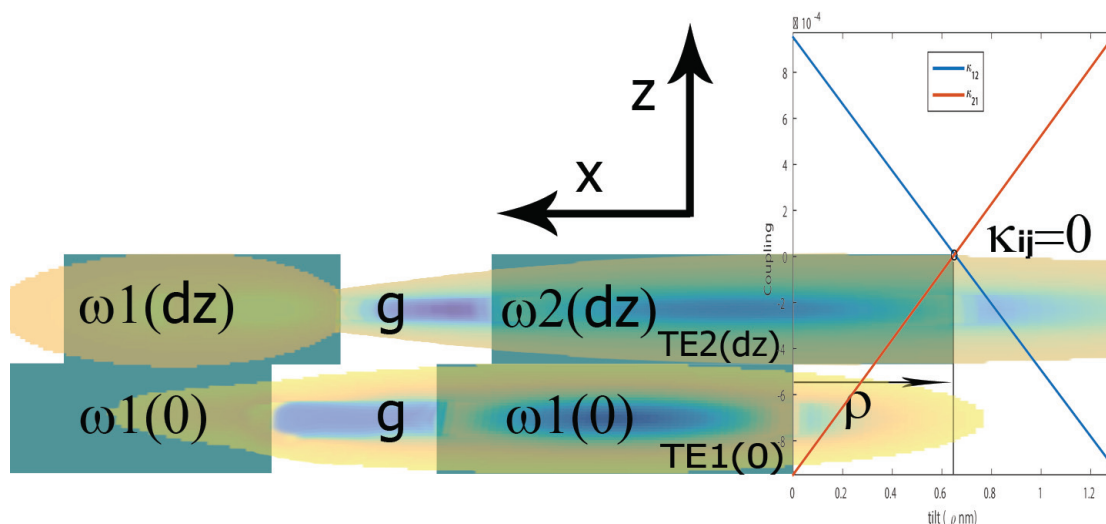


FIGURE 3.36: This figure is key to understand this last section. We can see on the background the two first layers of our design. Both layers have different width because the widths change with z . We are showing the first mode on the first section and the second mode on the second section. The overlap integral between those two modes and a term considering the variation on the dielectric from section one to section two gives us κ_{12} . Then we can move the second layer an amount ρ to the right. There is a ρ_0 where the $\kappa_{12} = \kappa_{21} \approx 0$

Notice that the coupling in one layer only depends on the layer right before. We can repeat this process until the last section ends. After doing that we will have found and we will be able to generate the zero coupling region.

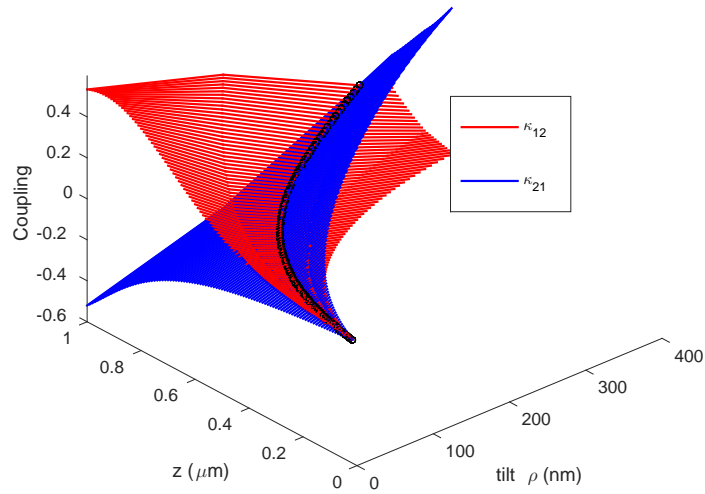


FIGURE 3.37: Coupling coefficients κ_{12} and κ_{21} versus tilt versus tilt and length. We can find the zero coupling condition for each length ($\rho_0(z)$).

Once we have $\rho_0(z)$ we can simulate the structure performance using the FMM code. As we can see, even though we found the intersection for the two surfaces κ_{12} and κ_{21} , that condition does not lead to zero coupling. However it minimizes the coupling.

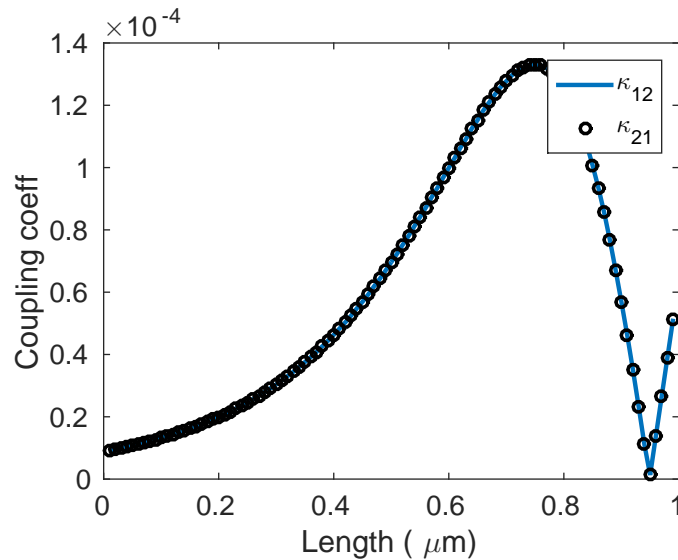


FIGURE 3.38: Coupling coefficients κ_{12} and κ_{21} versus normalized length.

If we do the simulation for a adiabatic structure with the same exact geometry of our structure but with $\rho(z) = 0 \forall z$ we needed a length of at least $\sim 200 \mu\text{m}$. Now the length is going to be $\sim 7 \mu\text{m}$.

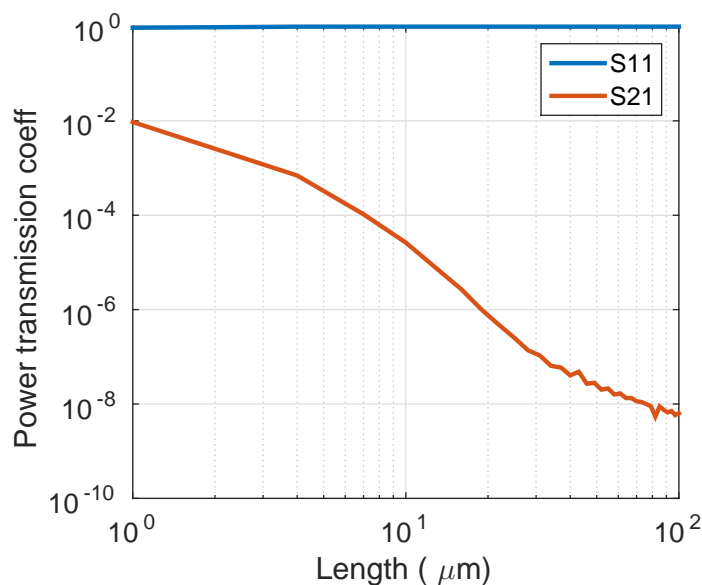


FIGURE 3.39: Power transferred from mode one to mode one and power transferred from mode one to mode two versus length of the device.

Now we want to verify our designs using FDTD. We will start with a two dimensional design since it takes less computational time and then we will do the three dimensional simulation. The geometry of the two dimensional design has been chosen analogously to the three dimensional.

As it happened with the directional coupler apart from the coupling region we need input and output waveguides. The output waveguide is easy to design and can be short since the only requirement is to have symmetry. The only thing we have to worry about is the curvature of the waveguides. If the bending is really abrupt they are going to scatter all the light.

The input starts with two equal singlemode waveguides separated by $\sim 0.8\mu\text{m}$. We have to link up this first layer with the first section of our coupling region. In the input region we will be changing gap and both widths. Again we could use an adiabatic structure to do this transition but does it not make sense since we want a short structure. The strategy that we are going to follow to design this part is similar to the one we used for the coupling region. We are going to define θ as the tilting of all the structure. So we are going to think about the input as a rigid piece that can rotate an angle θ . If we simulate the structure for different angles using FDTD2D we can see that there exists an angle that minimizes the coupling between crossed modes. Even more the parameter S_{12} is less than $1e-4$ which is desired. We will not be able to use this strategy in 3D since the minimum S_{12} we can achieve is $1e-3$ which means that assuming that everything works ideally besides the input part the maximum we can achieve is 40/60 at the output.

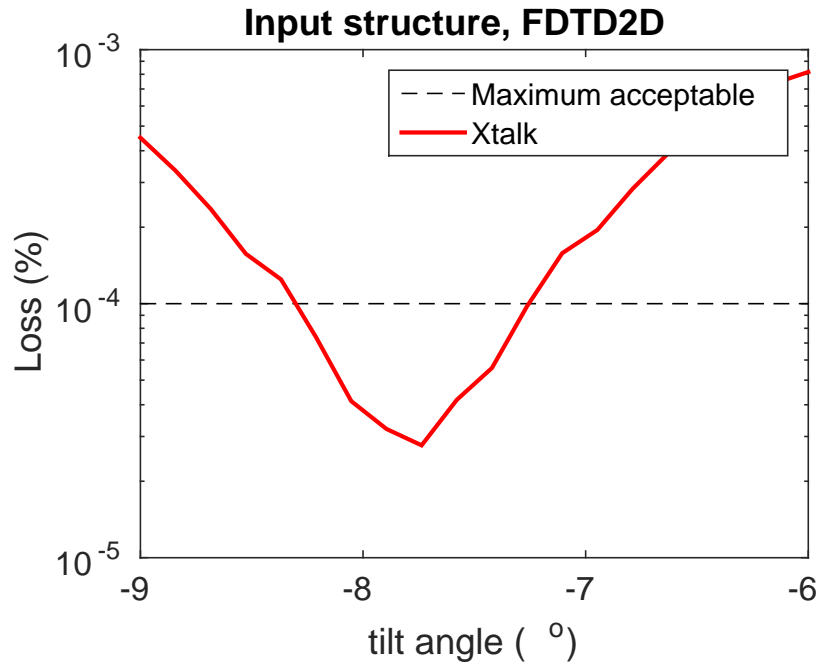


FIGURE 3.40: .

As we can see in FIGURE 3.40 we want an input angle about -8 degrees. Once the input is working the design the output in the same way as the directional coupler. So we just need two symmetrical sinusoidal bends.

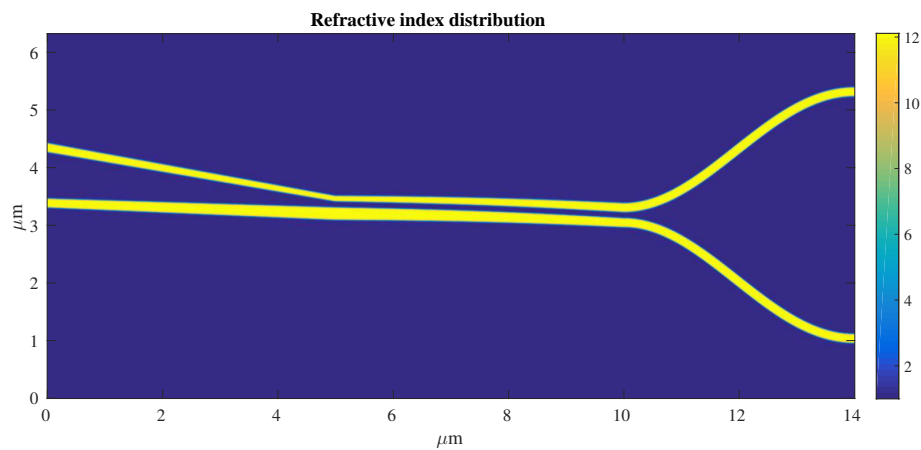


FIGURE 3.41: Left to right: Input region, coupling region and output region.

Then we fix the input and output size and we simulate the structure while changing the coupling region length.

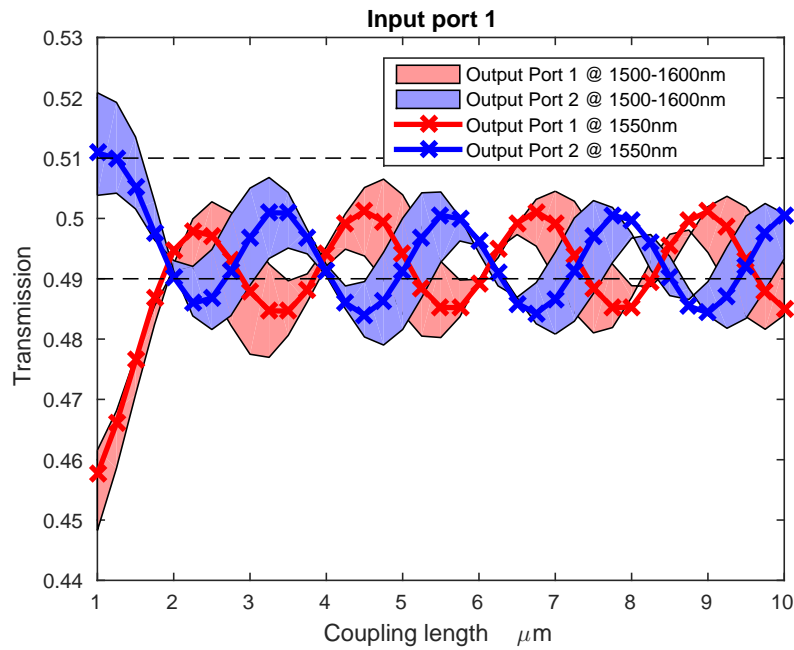


FIGURE 3.42: Coupler performance versus length latching the pulse on the upper waveguide.

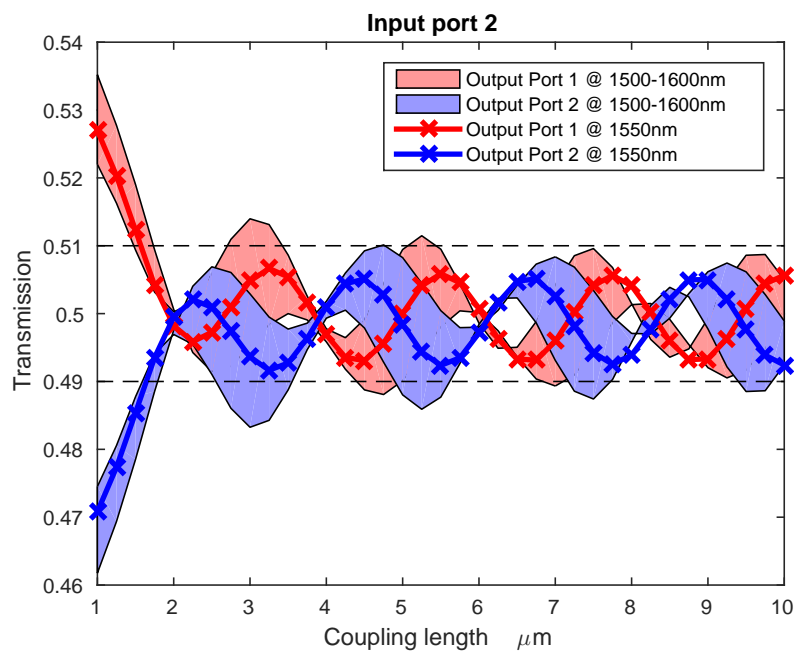


FIGURE 3.43: Coupler performance versus length latching the pulse on the down waveguide.

The results are promising. They oscillate with length and we can see that $L_{coupling} = 2\mu m$ gives a awesome performance.

The next step is designing a three dimensional structure. We could think that changing from 2D to 3D is straightforward but is not. In 3D we find some problems that we had not in 2D. The first problem is the existence of two different polarizations that can couple. We already solved this problem by using SiO₂ cladding. But doing that we reduced the index contrast and our design is not going to be as good. The second problem is the small gap required in 3D. This small gap yields a symmetrical mode where a lot of power is confined in the slot. Then if we are not careful when we separate the two waveguides at the output a lot of power will be radiated. We realized that going from 2D to 3D is not straight forward. So a three dimensional design will not be presented in this thesis but I will continue with that during my Ph. D. next fall 2016.

Chapter 4

Conclusions

I had two main aims in this thesis. Firstly I wanted to get a good understanding of the state of the art in quantum integrated photonics. My time was limited and I did my best to learn as much as possible about the topic. However, I think I still have a lot of papers to read and explore. I was not expecting to learn all about quantum integrated photonics in 10 months since I will have plenty of time to do that the next fall during my Ph.D. I want and I will continue my research on quantum integrated photonics and I would like to be one of the contributors for the first quantum computer.

Secondly, I proved a high performance beam splitter in 2D with a coupling region of $2\mu m$. Despite, I got good results in 3D; coupling region of $24\mu m$ I need more time to find clever ways to reduce the device length. The results until now have been really promising and a good design is going to come soon.

To sum up, during the last 10 months I have been learning a lot of new concepts and I have been solving new problems constantly. I had bad times and good times. I had a lot of frustrating weeks where nothing was working. That made me grow emotionally and intellectually. I feel like the person that arrived at Boulder the last July 27th of 2015 is not the same person that will leave Boulder on June 15th of 2016.

Bibliography

- [1] W. H. Zurek, 2003 *arXiv:quant-ph/0306072*
- [2] P. Shadbolt, *Complexity and Control in Quantum Photonics* (Springer , London, 2016)
- [3] D. Bonneau, J. W. Silverstone, M. G. Thompson *Chapter 2 Silicon Quantum Photonics* (Springer-Verlag , Berlin Heidelberg, 2016)
- [4] W. R. Clements, P. C. Humphreys, B. J. Metcalf, W. S. Kolthammer, I. A. Walmsley ,2016 *arXiv:1603.08788*
- [5] M. Reck, A. Zeilinger, H. J. Bernstein, P. Bertani *Phys. Rev. E* **73** 58 (1994)
- [6] S. Aeronson, A. Arkhipov ,2010 *arXiv:1011.3245*
- [7] G. N. Gol'tsman, O. Okunev, G. Chulkova, A. Lipatov, A. Semenov, K. Smirnov, B. Voronov, and A. Dzardanov; Picosecond superconducting single-photon optical detector; *Applied physics letters*, volume 79, number 6, (2001)
- [8] Michalet X, Colyer RA, Scalia G, Ingargiola A, Lin R, Millaud JE, Weiss S, Siegmund OHW, Tremsin AS, Vallerga JV, Cheng A, Levi M, Aharoni D, Arisaka K, Villa F, Guerrieri F, Panzeri F, Rech I, Gulinatti A, Zappa F, Ghioni M, Cova S. 2013 Development of new photon-counting detectors for single-molecule fluorescence microscopy; *Phil Trans R Soc B* 368: 20120035. <http://dx.doi.org/10.1098/rstb.2012.0035>
- [9] Chandra M Natarajan, Michael G Tanner and Robert H Hadfield; Superconducting nanowire single-photon detectors: physics and application; IOP publishing; *Supercond. Sci. Technol.* 25 (2012) 063001 (16pp)
- [10] Alex D. Semeov, Gregory N. Gol'tsman, Alexander A. Korneev; Quantum detection by current carrying superconducting film. *Physica C* 351, 349-356 (2001)
- [11] F. Marsili, V. B. Verma, J. A. Stern, S. Harrington, A. E. Lita, T. Gerrits, I. Vayshenker, B. Baek, M. D. Shaw, R. P. Mirin and S. W. Nam; Detecting single infrared photons with 93% system efficiency; *Nature Photonics* 7, 210–214 (2013)
- [12] Yamashita T, Miki S, Makise K, Qiu W, Terai H, Fujiwara M, Sasaki M and Wang Z Origin of intrinsic dark count in superconducting nanowire single-photon detectors *Appl. Phys. Lett.* 99 161105 (2011)
- [13] Tanner M G Enhanced telecom wavelength single-photon detection with NbTiN superconducting nanowires on oxidized silicon *Appl. Phys. Lett.* 96 221109 (2010)

-
- [14] D. Marcuse, *Theory of Dielectric Optical Waveguides* (Quantum electronics, Principles and Applications , Second Edition, 1991)
- [15] R. C. Rumpf, *Coupled-Mode Theory* (ECE 5322 21st Century Electromagnetics, <https://www.youtube.com/watch?v=pZalesCCPo>)
- [16] L. Chrostowski, M. Hochberg, *Silicon Photonics Design* (Cambridge University Press , Cambridge, 2015)
- [17] W.K. Burns, A.F. Milton *Waveguide Transitions and Junctions* (Chapter 3, Springer Series in Electronics and Photonics, volume 26, 1988)
- [18] M. Nielsen and I. Chuang, *Quantum Computation and Quantum Information* (Cambridge University Press, 1999).
- [19] R. Raussendorf, H. J. Briegel *Phys. Rev. E* **85** 22 (2001)
- [20] E. Knill, R. Laflamme, G. J. Milburn *Nature* **409**, 46-52 (2001)
- [21] T. C. Ralph, A. G. White, W. J. Munro, and G. J. Milburn, *Phys. Rev. E* **65** 012314 (2001)
- [22] T. C. Ralph, N. K. Langford, T. B. Bell, and A. G. White, *Phys. Rev. E* **65** 062324 (2002)